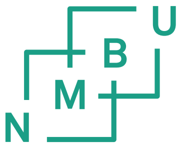

Norwegian University of Life Sciences
Faculty of Environmental Science and Technology
Department of Mathematical Sciences and Technology

Master Thesis 2014
30 credits

Hyperspectral Photoluminescence Scans of mc- Si Wafers Analysed through Multivariate Curve Resolution (MCR)

Astrid Kristine Fremme

Preface

This thesis is part of an on-going research project at the Norwegian University of Life Sciences (NMBU).

I would like to thank my three supervisors; Espen Olsen, Ingunn Burud and Andreas Flø for all helping me understand the physics better and teaching me how to write a master's thesis. I further want to thank my mother and Marie for proof reading. And most of all I would like to thank Marius for being there throughout the whole process and supporting me in every way.

With this thesis I conclude my master's degree in Environmental Physics and Renewable Energy at the Norwegian University of Life Sciences (NMBU).

Ås, May 14, 2014
Astrid Kristine Fremme

Abstract

Characterisation of defects in solar cell material is one step towards higher energy conversion efficiency of solar cells. The method used in this study allows detection across the wafer of defects causing radiative SRH recombination.

In this experiment 30 unpassivated, full size mc-Si wafers from three different ingots are cooled to 90K. Emissions after excitation with a 808 nm laser are detected by scanning the samples with a hyperspectral camera recording in the range 900-2500 nm, which includes both band-to-band photoluminescence (BB-PL) and defect related luminescence (DRL).

Multivariate Curve Resolution (MCR) statistical analysis is used to separate the recorded emission into different signals. Even though surface recombination greatly influences the results, eight different signals were found for the most signal-rich wafers from one ingot (B2). Although all samples from one ingot are believed to contain the same types of defects, emissions were only separated into a few signals for the most defect-rich samples. Wafers from the B2 ingot are standard mc-Si wafers, with both grain size and number of emission signals successfully differentiated increasing with increasing height on the ingot. The wafers from the two other ingots are HPM Si wafers, and are more stable in respect to both grain size and number of signals differentiated from wafers from different heights on the ingot. Emission signals were identified as being of specific energy, but they were not always distinctively coupled with emission signals from literature.

Sammendrag

Karakterisering av defekter i solcellemateriale er et steg mot høyere effektivitet i solceller. Metoden brukt i denne studien gir muligheten til å finne defekter som forårsaker radiativ SRH rekombinasjon i områder på waferen.

I dette eksperimentet er 30 upassiverte mc-Si wafere i full størrelse fra tre forskjellige støpeblokker kjølt til 90K. Etter eksitasjon med en laser (808 nm), blir utstråling målt ved å skanne prøvene med et hyperspektralt kamera med følsomhet i området 900 – 2500 nm, som inkluderer både bånd-til-bånd fotoluminisens (BB-PL) og defektrelatert luminisens (DRL).

Statistisk multivariat analyse (MCR) er brukt for å skille den målte utstrålingen i ulike signaler. Selv om overflaterekombinasjon har stor innvirkning på resultatene, ble åtte ulike signaler funnet for wafere fra støpeblokk B2 med flest forskjellige signaler. Selv om alle wafere fra en strøpeblokk antas å inneholde de samme typer defekter, ble utstrålingen bare delt inn i et få antall signaler for prøver med høyt defektinnhold. Wafere fra B2-blokken er standard mc - Si wafere, med både kornstørrelse og antall unike signaler økende for økende høyde i blokken. Wafere fra de to andre blokkene er HPM Si wafere, og er mer stabile i forhold til både kornstørrelse og antall forskjellige signaler funnet ved forskjellige høyder i blokken. Signalene ble identifisert til å ha en spesifikk energi, men de var ofte ikke mulig å definitivt koble et målt signal med et kjent signal fra litteraturen.

Contents

List of abbreviations and symbols .... **vi**

List of Tables .... **vi**

List of Figures .... **vii**

1 Introduction **1**

2 Theory **3**

2.1 Production of Silicon Solar Cells 3

2.2 The Atomic Structure of Crystalline Silicon and Defects 4

2.2.1 Doping 6

2.3 Band Model and Excitations 6

2.4 Phonons 8

2.5 Inter Band Gap Energy Levels 9

2.6 Recombination Mechanisms 9

2.6.1 Radiative Band-to-Band Recombination 10

2.6.2 Auger Recombination – Non Radiative Band-to-Band Recombination 10

2.6.3 Shockley Read Hall Recombination 11

2.6.4 Surface Recombination 12

2.7 Recording Photoluminescence 14

3 Literature study **15**

3.1 Efficiency Estimates for Unpassivated Wafers 15

3.2 Defect Related Luminescence (DRL) Lines 16

3.3 Origin and Cause of DRL Signals 17

3.4 Temperature Dependency 17

3.5 Summary Table 19

4 Experimental Setup and Data Processing **20**

4.1 The Wafer Samples 20

4.2 Equipment Description 21

4.2.1 Movable Rig 21

4.2.2 Cryogenic Cooler 22

4.2.3 Laser 23

4.2.4 Camera and Filter 23

4.2.5 Computer Programs 26

4.2.6 Other ... 26
4.3 Equipment Setup and Data Collection ... 27
4.3.1 Cooling with Liquid Nitrogen ... 27
4.3.2 Moving the Wafers ... 27
4.3.3 Operating Laser and Camera ... 28
4.3.4 Additional Images ... 28
4.4 Data Processing ... 29
4.4.1 MATLAB ... 29
4.4.2 Solo+MIA 7.5.2 ... 29
4.4.3 Adobe Photoshop CS5 and Fiji ImageJ 1.48a ... 30
5 Results and Discussion ... 31
5.1 Detailed Results for Wafer B2_053 at 90K ... 31
5.1.1 Analysis of Emissions by Using MATLAB to Extract Images ... 31
5.1.2 MCR Analysis Results for wafer B2_053 ... 37
5.2 Comparing Wafers from Different Heights in an Ingot ... 45
5.2.1 Comparison of Emission Signals across the B2 Set of Wafers ... 45
5.2.2 Comparison of MCR Components across Wafers in the B2 Set ... 47
5.2.3 Comparison of MCR Components across Wafers in the A2+C and HM Sets ... 61
5.3 Comparison between Ingots ... 64
5.4 Room Temperature and RGB Images ... 66
5.4.1 Room Temperature Images ... 66
5.4.2 RGB Image and Comparison with emission signals ... 66
6 Conclusion ... 67
6.1 Further Research ... 68
References ... 69
Appendix ... 71
A. RGB Images of Fist and Last Wafers in each wafer set ... 71
B. Example of Components Showing Noise for Wafer B2_053 ... 75
C. Images Showing Component Pairs for Wafer B2_053 ... 76
D. Tables of Values in Figures 5.13, 5.26, 5.27 ... 79
E. Comparison of Emission Signals and Positions on Wafers ... 80
E.1. Wafer B2_005 ... 80

E.2. Wafer B2_092 81

List of abbreviations and symbols

ARC	Anti-reflection coating
BB	Band-to-band
Cu	Copper
DRL	Defect Related Luminescence
Ec	State in conduction band with lowest energy
Ev	State in valence band with highest energy
Fe	Iron
HPM	High Performance Multicrystalline
IR	Infrared
Isc	Short circuit Current
mc	Multicrystalline
Mn	Manganese
PCA	Principal Component Analysis
PL	Photoluminescence
PV	Photovoltaics
sc	Single crystalline
Si	Silicon
Ti	Titanium
Voc	Open circuit voltage

List of Tables

Table 3.1: Summary of some reported emission lines.. 19
Table 4.1: List of wafers analysed 21
Table 4.2: Centre energy of each band recorded by the camera [eV]................................... 24
Table 0.1: Band number of loadings peaks in B2 set 79
Table 0.2: Band number of loadings peaks in A2+C set. 79
Table 0.3: Band number of loadings peaks in HM set.. 79

List of Figures

Figure 2.1: The atomic structure of silicon/ electron bonding model 4
Figure 2.2: Electron bonding model of Silicon showing excitation of one electron. 5
Figure 2.3: Doping Silicon with Phosphorous. 6
Figure 2.4: Energy band model for an undoped semiconductor. 7
Figure 2.5: Band model for indirect semiconductor. 8
Figure 2.6: Energy levels in the band gap introduced by impurities in Silicon 9
Figure 2.7: Band-to-band recombination in an indirect semiconductor 10
Figure 2.8: Auger recombination 11
Figure 2.9: Shockley Read Hall recombination.. 12
Figure 2.10: Surface recombination 13
Figure 4.1: Equipment used in this experiment 22
Figure 4.2: Aluminium plate used when finding temperature 23
Figure 5.1: Montage of each separate band for wafer B2_053. 34
Figure 5.2: Five images of the B2_053 wafer at selected energies. 35
Figure 5.3: Detected emissions from wafer B2_053 with certain energies............................ 36
Figure 5.4: Finding VID3 for wafer B2_053 by subtraction 36
Figure 5.5: Scores image for component 1 from MCR analysis of wafer B2_053 38
Figure 5.6: Loadings plot for component 1 from MCR analysis of wafer B2_053 39
Figure 5.7: Scores images for each component from the MCR analysis result for wafer B2_053.. 40
Figure 5.8: Loadings plots for separate MCR components for wafer B2_053. 41
Figure 5.9: Loadings plot of significant components for wafer B2_053. 42
Figure 5.10: Components for wafer B2_053 and predetermined emission lines 44
Figure 5.11: Signals at selected energies for wafers in the B2 set.. 45
Figure 5.12: Number of components obtained for wafers in the B2 set 47
Figure 5.13: Peaks on loadings plots from MCR analysis results of B2 wafers 48
Figure 5.14: Colour code for figures showing signals from different wafers.......................... 49
Figure 5.15: Loadings plots of components for B2-wafers, peak at bands 30-33 50
Figure 5.16: Loadings plots of components for B2 wafers, tall peaks at bands 50-52 and 58-59 51
Figure 5.17: Loadings plots of components for B2 wafers, peak at bands 62-63................... 52
Figure 5.18: Loadings plots of components for B2 wafers, peak at bands 66-68................... 53
Figure 5.19: Comparison of components at bands 62-63 with those at bands 66-68............ 54
Figure 5.20: Loadings plot of components for B2 wafers, peak at bands 76-84 55
Figure 5.21: Loadings plot of components for B2 wafers, peak at bands 90-97 56
Figure 5.22: Comparison of components at bands 76-84 with those at bands 90-97............ 57
Figure 5.23: Loadings plot of components for B2 wafers, peak at bands 100-110. 58
Figure 5.24: Loadings plot of components for B2 wafers, peak at bands 120-130 59
Figure 5.25: Summary of emission signals identified in B2 wafers... 60
Figure 5.26: Peaks on loadings plots from MCR analysis results of A2+C wafers................... 61

Figure 5.27: Peaks on loadings plots from MCR analysis results of HM wafers 62
Figure 5.28: Number of significant components in the different sets.................................... 64
Figure 5.29: Loadings plots peaks from MCR analysis results of wafers in three sets. 65
Figure 0.1: RGB image of wafer B2_005. 71
Figure 0.2: RGB image of wafer B2_092. 72
Figure 0.3: First and last wafer in A2+C set.. 73
Figure 0.4: First and last wafer in HM set 74
Figure 0.5: Scores for components showing noise 75
Figure 0.6: Component pairs for wafer B2_053 (1) 76
Figure 0.7: Component pairs for wafer B2_053 (2) 77
Figure 0.8: Component pairs for wafer B2_053 (3) 78
Figure 0.9: MATLAB extracted emissions overlaid on one image of wafer B2_005................ 80
Figure 0.10: Scores images overlaid on RGB images of wafer B2_005................................... 80
Figure 0.11: MATLAB extracted emissions overlaid on image of wafer B2_005..................... 81
Figure 0.12: MATLAB extracted emissions overlaid on one image of wafer B2_092.............. 81
Figure 0.13: Scores images overlaid on RGB images of wafer B2_092................................... 81

1 Introduction

We have many reasons to encourage the increased use of renewable energy, like environmental benefits and energy security. Renewable energy has the capacity of providing us with energy at minimal costs of degradation to the environment, and it has the added promise of also being available in the far future. On the other hand, renewable energy brings its own difficulties, which in some cases are large enough to be barriers to their continued use and development. Sometimes a technology's efficiency is limited and the availability of energy cyclical or unreliable, requiring the use of more land resources and energy reserves than would be necessary with other types of technologies. However, the prices of fossil fuels keep rising, and the prices of renewables keep sinking, thus making the use of renewable energy more attractive.

Every day the Earth receives an incredible amount of energy from the Sun, and 0.01% of the energy reaching the Earth would be enough to satisfy the energy need of the world.[1] One of the most direct ways to convert this energy into electricity is by using solar cells, in which single- and multicrystalline silicon cells are the most common.

Crystalline silicon solar cells are made of very pure silicon. Multicrystalline silicon (mc-Si) requires less processing, making it cheaper to produce. However, it also contains more impurities and imperfections that reduce the cells' efficiency. Identification and better understanding of these imperfections are the first step in improving the cells' efficiency. Ideally we'd like to be able to detect and differentiate the different types of defects, know what can be done to diminish them, their influence and acceptable levels.

In the past, measurements have mostly been done with either spectral or spatial resolution. The strength of the experiments conducted for this thesis is that they have both high spatial and spectral resolution.

This thesis deals with hyperspectral photoluminescence (PL) scans performed on unpassivated silicon wafers. The scans are analysed using Multivariate Curve Resolution (MCR) and sorted into separate emission signals with corresponding distributions on the wafers. In combination with other types of measurements (like measurements of concentration of a particular impurity) and other types of information (like details on the wafer production method) studies similar to the one conducted here could give valuable information as to what causes these defects and how to avoid them.

From the literature study we can see that PL scans on unpassivated wafers may let us know the defective areas of a wafer. The hyperspectral PL imaging will in this thesis be used as a diagnostic tool for defect analysis rather than for finding efficiency estimates, as is

sometimes done. At this stage conclusions cannot yet be made on the mechanisms behind emission signals.

The study of this thesis tries to find and separate different emission signals. Questions to be answered are:

Which defect emission signals can be detected and separated from the rest?
What energies do the detected emission signals have?
What characteristics do these emissions have?
Which DRL lines from literature might they correspond to?
Are there any differences in emission signals from different wafers and ingots?

This thesis is built up by 6 different chapters with this introduction being the first chapter. A theoretical background, a literature study and details on the experiment are presented in chapters 2, 3 and 4 respectively. Chapter 5 presents results and discussion, and chapter 6 a conclusion and suggestions for further research.

2 Theory

The experiments conducted in this study were done with multicrystalline (mc) "as-cut" silicon (Si) wafers. "As-cut" means they are in the process step where they have just been sawed to slices from the ingot. They still have several steps left before becoming finished solar cells. Crystalline silicon has characteristics ideal for solar cell manufacturing. However, mc-Si contains numerous defects which diminish a solar cell's production output.

2.1 Production of Silicon Solar Cells

Silicon (Si) has become the most extensively used semiconductor in solar cells. It is readily available as a common element on the Earth's crust as sand and its characteristics fit well with incoming radiation on the Earth from the Sun. [1, 2]

The first step towards making solar cells is producing metallurgical grade Si (98% pure) out of quartz sand. Then the Si is taken through one or several processes to purify it further (at least 99.9999% pure).[1] The Siemens process has existed for a long time, and requires a large amount of energy and has a low yield. [1] A newer process is the REC process, which consumes less energy and has a higher yield. [1]

The silicon can then be melted, doped[1] and solidified to make ingots. The silicon can be crystallized into single- or multicrystalline ingots, depending on the solidification process. Single crystalline (sc) ingots can be made through the Czochraski process or the float-zone process. Mc-Si can be made through melting and solidification. [1]

The silicon ingots are then sliced into wafers, losing about half of the material as cut losses. At this stage the wafers are so-called "as-cut" wafers. They then go through a series of processes where the wafers' surfaces are doped again, polished, etched, passivated, textured, coated and are attached metal contacts. The wafers are then joined and encapsulated into glass and metal modules.[1, 2]

Making sc ingots require both energy-intensive and costly processes, which give rise to a price difference between mc-Si and sc-Si solar cells. [1] However, sc-Si silicon solar cells will generally be more efficient. [1, 2]. There also exist alternative ways to make wafers, for example by making ribbon silicon. But these are not cost effective.[2]

[1] Doping is explained in the next chapter.

2.2 The Atomic Structure of Crystalline Silicon and Defects

In crystalline silicon, the atoms are aligned in a complicated, but orderly manner. A common simplification is to represent this structure as a grid of atoms connected by shared electrons, covalent bonds, as shown in Figure 2.1. Silicon atoms have 4 electrons in their outer shell, and 4 free spaces that are filled by neighbouring atoms. When every electron is shared by two atoms and all atoms get a full outer shell, the electrons are in their ground state. When a bond breaks an electron-hole pair is made, which means there is both a spare electron somewhere and an electron missing somewhere else, as shown in Figure 2.2. A hole is the potential to hold an extra electron. [3]

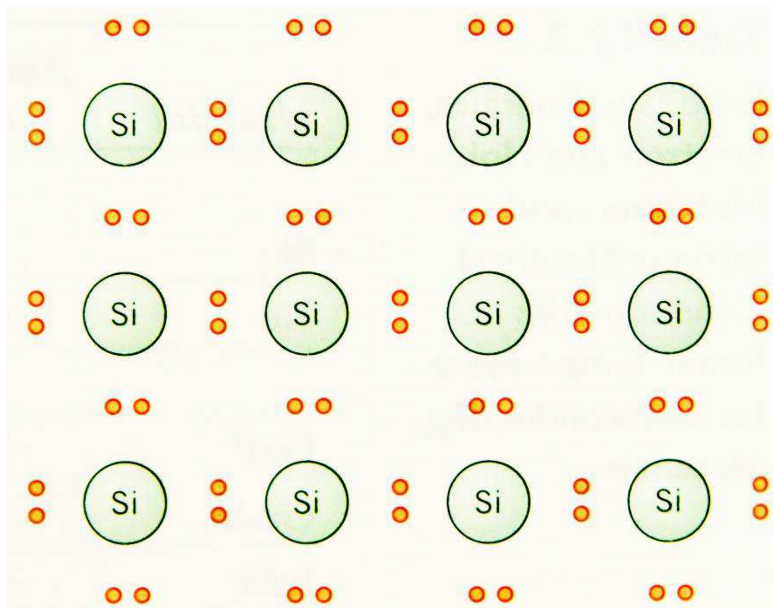

Figure 2.1: The atomic structure of silicon/ electron bonding model
Circles marked Si represent silicon nuclei and their filled shells, while the small circles are electrons in outer shells. Each silicon atom contributes with four electrons and shares them in covalent bonds. [3]

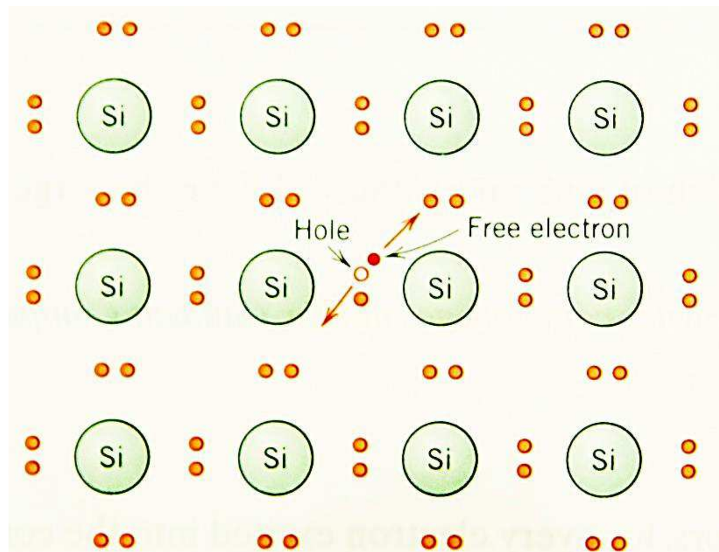

Figure 2.2: Electron bonding model of Silicon showing excitation of one electron. *An electron-hole pair is generated, now both the electron and the hole can move around. [3]*

Multicrystalline Si is made up of many smaller crystals, and thus contains more defects. Defects can be categorized into four types, which are point, line, surface and volume defects.

Point defects can either be intrinsic or extrinsic. Intrinsic point defects are either a vacant atomic site, or a self-interstitial atom. A vacant site means one of the Si atoms in Figure 2.2 is missing. A self-interstitial atom means there is one extra Si atom in the orderly lattice of Si atoms. Intrinsic point defects are dependent on temperature, and are more probable at higher temperatures. Extrinsic point defects are impurity atoms, which can be either substitutional or interstitial. Substitutional impurity atoms are atoms of a different element which take the place of one Si atom in Figure 2.2. This happens when doping the material. Interstitial impurity atoms are atoms of a different element which exist in the orderly lattice of Si atoms. Both intrinsic and extrinsic interstitial atoms can cause distortions in the surrounding lattice. [4]

Surface or planar defects can be caused by stacking faults, which means that the pattern of atomic arrangement is interrupted along a surface. Furthermore, there are grain boundaries, which are the boundaries between single crystals with different stacking direction. The misorientation angle between bordering grains can be either small or large. Impurities tend accumulate at crystal borders.[2] Twin boundaries also exist where the structure of one original crystal continues across the boundary, but with a new direction.[4]

Line defects include dislocations. Dislocations can be an edge or a screw dislocation line. Volume defects are precipitates, voids and bubbles. [4]

2.2.1 Doping

In the process of making solar cells, introduction of non-silicon material is done on purpose to exploit the effects these have on the semiconductor. Impurity atoms with one more (Group IV, n-doping) and one less (group III, p-doping) electron in the outer shell compared to Si are used; a model is shown in Figure 2.3. The material is then called p- and n-material respectively. The doping concentration is very low, so each impurity atom will for the most part only be surrounded by Si atoms.

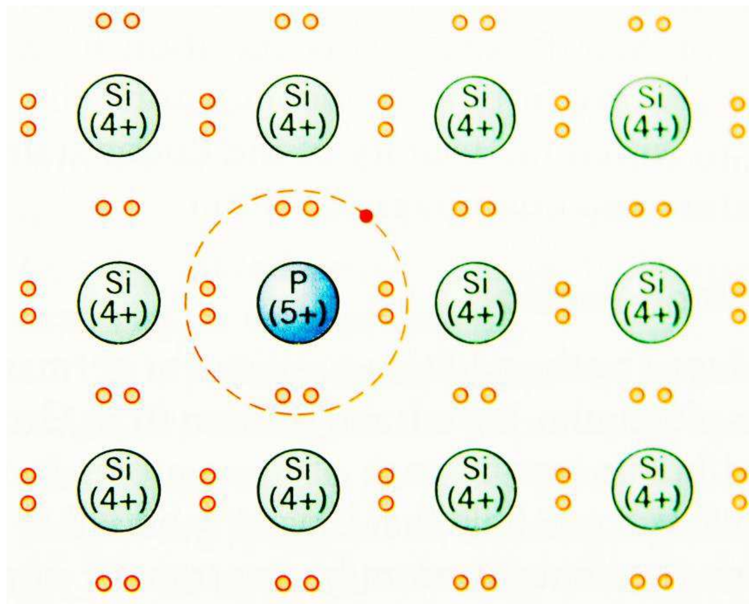

Figure 2.3: Doping Silicon with Phosphorous.
The phosphorous (P) atom substitutes a Silicon atom and contributes with one extra electron in its outer shell. The extra electron will be free at room temperature. [3]

When p- and n- material interact, the extra, unbound electron in the n-material will diffuse into the p-material over what is called the diffusion layer. Thus the left over material will be net positively (n-material) or negatively (p-material) charged, creating a stable electric field which is then used to gather free electrons excited by incoming photons from the sun, thus creating electrical current from incoming sunlight. [1, 3]

2.3 Band Model and Excitations

Band diagrams are used to describe the available energy levels for an electron in the Si outer shell. Figure 2.4 (a) shows a simple band diagram for a semiconductor with no defects, with the conduction band, the band gap and the valence band. The valence and conduction bands represent allowed energy levels, while an energy level inside the band gap is forbidden. When electrons are in their bound, ground state, they have energy corresponding to a place in the valence band. When an electron is free it is excited and is in the conduction band. When an electron moves into the conduction band it leaves a hole in the valence band as

shown in Figure 2.4 (b). A hole can be treated as a positively charged particle which also participates in electronic conduction. [3]

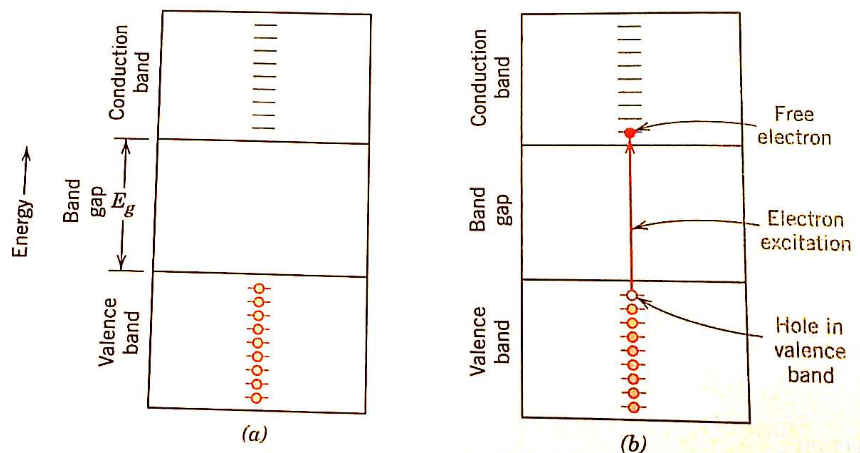

Figure 2.4: Energy band model for an undoped semiconductor.
(a) is before electron excitation, and (b) is after excitation. When an electron moves from the valence band to the conduction band, a hole is also created in the valence band. The band gap contains no allowed energy states in a semiconductor without defects. Not to scale[3]

An electron can be excited through different mechanisms. One is thermal excitation, where Fermi–Dirac statistics provide an equation for the number of electrons in the conduction band. [1] Electrons can also be excited through the absorption of incoming photons. If an incoming photon has energy more than or equal to what is needed to make the jump into the conduction band, the electron absorbs the photon's energy and is excited up into the conduction band. This corresponds to breaking a covalent bond and making an electron-hole pair, which can then move around. The size of the band gap is different for different materials. In metals it is non-existent, in semiconductors it is in the range 1-2 eV, and for insulators it is larger than 2 eV. For undoped silicon the band gap energy in room temperature is 1,12 eV. At lower temperatures, the size of the band gap increases, but with doping it decreases.[3] [1]

A larger band gap means more electricity out of the solar cell per absorbed photon, but if the photon has less energy than the size of the band gap it will not be absorbed. There is a balance between wanting a large gap to be able to harvest a large amount of energy per absorbed photon and small enough band gap to be able to absorb more photons. A way to take better advantage of high energy photons while not losing low energy photons is to use multijunction tandem solar cells. [1]

A photon's energy and its wavelength have the relationship:

$$E = \frac{hc}{\lambda}, \tag{1}$$

where E is the photon's energy, h is Planck's constant, c is the speed of light and λ is the photon's wavelength. High energy corresponds to a short wavelength. This relationship is used throughout this thesis for converting between wavelength and energy.

2.4 Phonons

Silicon is an indirect band gap semiconductor. This makes the concept of phonons important. While a photon is a "quantum unit of electromagnetic energy"[3], a phonon is a "single quantum of vibrational or elastic energy"[3]. While photons small momentum and large energy, phonons have large momentum and small energy. Phonons are needed when an electron recombines with a hole through an indirect semiconductor.

A band model for an indirect band gap semiconductor is shown in Figure 2.5. Here it can be seen that to be excited from the valence band into the conduction band the electron needs not only energy but also momentum. This momentum must be provided by phonons. Alternatively the electron can be excited to a position with the same momentum. To do this a much larger energy is necessary, and this process is therefore less probable. [2]

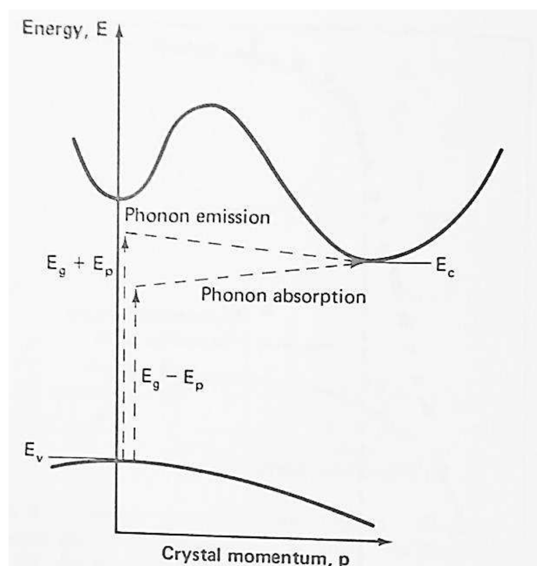

Figure 2.5: Band model for indirect semiconductor.
In an indirect semiconductor, an electron has to move from the state in the valence band with highest energy ('Ev') to the state in the conduction band with the lowest energy ('Ec') to be excited. The X-axis on the diagram shows changing crystal momentum, so to be able to move from 'Ev' to 'Ec' phonons have to be absorbed or emitted in order to change the momentum of the electron. [2]

2.5 Inter Band Gap Energy Levels

Defects in the material introduce allowed energy levels in the energy gap. Figure 2.6 shows some of the position of energy levels introduced by impurity atoms. In addition to these, other types of defects also introduce energy levels in the band gap.

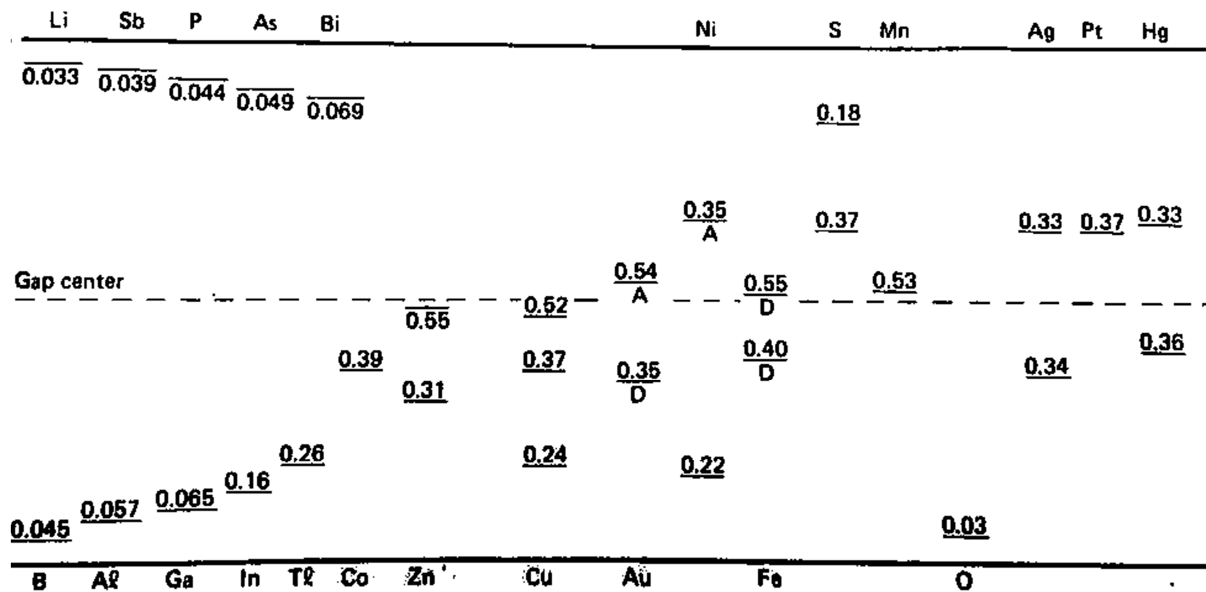

Figure 2.6: Energy levels in the band gap introduced by impurities in Silicon
This figure shows some of the energy levels introduced by selected impurities. Above the upper line lies the conduction band, and below the bottom line lies the valence band. The dotted line marks the centre of the band gap. [2]

Energy levels close to the gap centre have the most detrimental effect on finished cell performance. This means that some types of impurities are acceptable in larger quantities in the material than others. [2]

2.6 Recombination Mechanisms

Recombination of an electron and a hole can happen in several ways. Recombination corresponds to an electron going from the conduction band in Figure 2.4 down to the valence band and filling a hole there. It is known that defects deteriorate the efficiency of the finished cell. Defects act as recombination centres, hindering the purpose of the solar cell, which is to harvest these electrons.

There are two ways in which the electron can go directly from the conduction band to the valence band. One is through radiative recombination and the other is through the Auger effect. In addition to these there are two ways an electron can recombine non-directly;

these are the SRH mechanism and surface recombination. The total recombination rate is the sum of the individual recombination rates for each mechanism. [2]

2.6.1 Radiative Band-to-Band Recombination

After some time in the conduction band the electron might simply recombine with a hole in the valence band by emitting a photon corresponding closely with the energy difference and emitting or receiving phonons, as shown in Figure 2.7. As silicon is an indirect band gap semiconductor, additional phonons are required for the recombination process. Radiative band-to-band is therefore not a dominant recombination process for indirect semiconductors. [2]

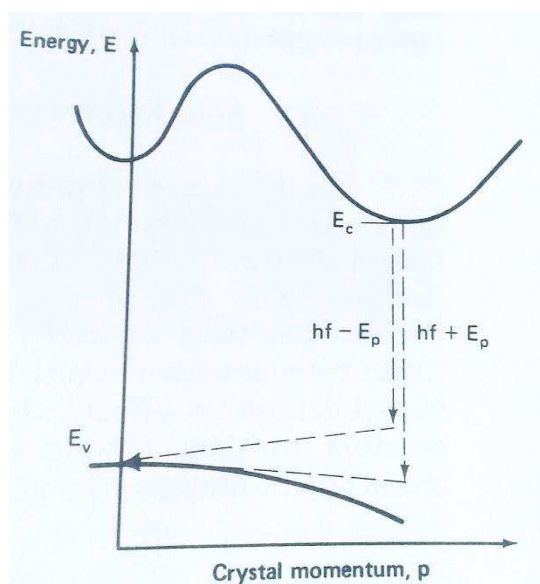

Figure 2.7: Band-to-band recombination in an indirect semiconductor
Above the upper, curved line lies the conduction band, and below the bottom curved line lies the valence band. This figure shows crystal momentum on the X-axis. 'Ec' marks the state on the conduction band with lowest energy. Excited electrons will move quickly to this state. 'Ev' marks the state on the valence band with the highest energy. The prefered band-to-band recombination mechanism is from 'Ec' to 'Ev'. As 'Ec' and 'Ev' have different momentum, phonons are needed for the recombination process. [2]

2.6.2 Auger Recombination – Non Radiative Band-to-Band Recombination

The second method for band-to-band recombination is called Auger recombination, and is non-radiative. Auger recombination is illustrated in Figure 2.8. It happens when an electron from the conduction band combines with a hole in the valence band by transferring its energy to either a second electron in the conduction band or a hole in the valence band. The second electron or hole will then transfer its excess energy to its surroundings by emission of

phonons. According to Green this process is mostly important for materials with high doping concentrations – over 10^{17} cm^{-3}. [2]

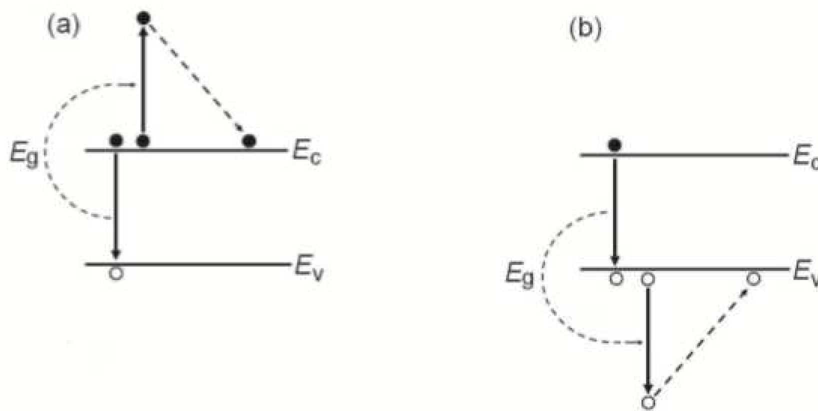

Figure 2.8: Auger recombination
'Ec' and 'Ev' mark the lowest energy for the conduction band and the highest energy of the valence band respectively. (a) shows an electron recombining with a hole by transferring its excess energy to a second electron in the conduction band. (b) shows the process happening by energy transfer to a hole in the valence band. The process is non-radiative when considering photons. [1]

2.6.3 Shockley Read Hall Recombination

The third recombination method for silicon material is the Shockley Read Hall (SRH) recombination process, which involves the use of energy levels introduced by impurities. SRH recombination is a multiple step process which can be both radiative and non-radiative. The process is illustrated in Figure 2.9, where an electron first loses energy either as heat or by emitting a photon with the energy corresponding to a drop to an energy level in the band gap. It can then continue to drop to the valence band either by emitting a second photon or by emitting more heat. A photon emitted this way has less energy than the height of the band gap, and therefore also a longer wavelength. This process can also include the electron going through more than one energy level in the band gap. [2]

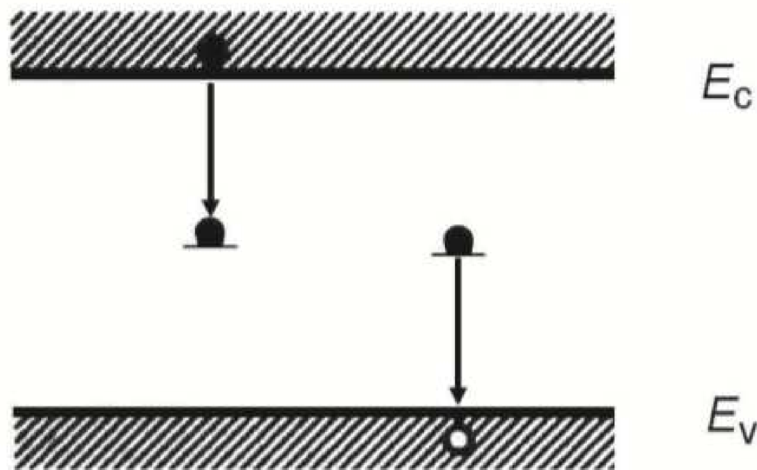

Figure 2.9: Shockley Read Hall recombination
The Shockley Read Hall (SRH) recombination mechanism takes place in multiple steps. An electron in the conduction band relaxes to an inter-band-gap energy level introduced by a defect. The electron then relaxes into the valence band. It might also go through more than one inter-band-gap energy levels. [1]

2.6.4 Surface Recombination

A fourth recombination method is surface recombination. It is illustrated in Figure 2.10. This recombination process is also caused by allowed states within the band gap. It is always non-radiative concerning photons. At the surface of the silicon material there are silicon atoms that don't have enough neighbouring atoms to allow its outer shell to be filled by electrons in covalent bonds. [3] These holes and unpaired electrons act as a large amount of inter-band gap energy levels. Recombination through these states becomes very efficient. Electrons can easily relax down into the valence band. [2]

In a finished cell, surface recombination is avoided by passivation – the application of anti-reflection coatings that take hold of these free bonds. [1]

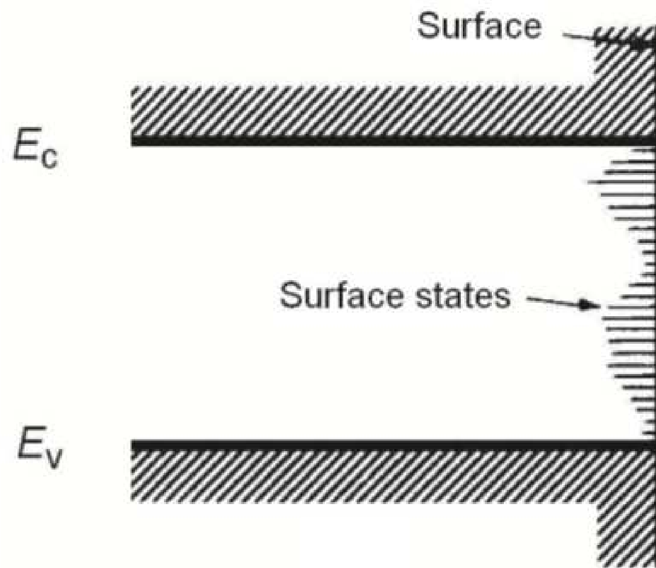

Figure 2.10: Surface recombination
The surface of the material constitutes a large number of defects, which introduce multiple energy states within the band gap. Electrons in the conduction band will relax to the valence band by going through these states. [1]

2.7 Recording Photoluminescence

Using a hyperspectral camera the photoluminescence (PL) emitted by the silicon wafer is measured. The PL signal comes from electron-hole pairs recombining through radiative recombination mechanisms. They emit photons with varying energy that we detect. Only emissions from radiative band-to-band (BB) recombination and radiative SRH recombination will be recorded. Other recombination mechanisms will influence our results, especially surface recombination, which will allow a large number of electron-hole pairs to recombine, causing the PL signal to have lower intensity.

When no levels inside the band gap are present (a good quality semiconductor) electrons will recombine with holes through the radiative BB recombination process or the non-radiative Auger recombination process. In a perfect quality semiconductor only PL from the BB recombination process would be visible. However, when the material contains defects that create energy levels in the band gap, a large number of electrons will instead recombine with holes through the SRH and surface recombination processes. Since surface recombination is non-radiative, in a highly defective area of a wafer it is emissions from the SRH recombination process which dominate. This is called defect related luminescence (DRL), and occurs in a lower energy range than BB-PL.

In Section 3.1 of this thesis, some examples of the use of BB-PL scans are shown. They are used to characterize the quality of unfinished wafers and solar cells.

DRL scans are also used for characterizing wafer material, but they have an additional use, as they allow us to distinguish between different signals. However, as can be seen in the Literature Study much is yet uncertain when it comes to DRL signals. Different signals are not easily distinguishable, and in some cases there is large uncertainty as to which defect causes which emission signal.

In the past, after doing measurements at a single point on a wafer, different signals were often separated by doing a Gaussian fit. Alternatively a scan was performed of a whole wafer, but with no spectral resolution. These types of measurements include less information than what we are able to extract.

The best known emission signals are the four D lines, D1, D2, D3 and D4, which occur at their respective energies, and are believed to be caused by dislocations. [5]

3 Literature study

This chapter presents a selection of published articles that are relevant for the interpretation of results obtained in this thesis. Most articles presented discuss somewhat different conditions than those for the study conducted for this thesis. Relevant literature includes articles on the effect of passivation, of the different signals' characteristics (like signal shape, energy of emission signals and temperature dependencies) and theories on the origin of these signals.

Photoluminescence (PL) measurements have been done on semiconductor material since the 1970s, but the mechanisms behind the emissions are still not completely understood, and the characteristics of different emission signals are still not clearly defined. There are uncertainties and disagreements, and as our understanding in this area improves, some of the older theories are disproved.

When reading this chapter it might be good to keep in mind that the measurements done for this thesis are performed on as-cut, unpassivated mc-Si wafers at low temperature (90 K) in the range 0.49 – 1.34 eV, which includes both the band-to-band photoluminescence (BB-PL) and defect related luminescence (DRL). Measurements done on other premises, though relevant, might show different results.

3.1 Efficiency Estimates for Unpassivated Wafers

Some authors claim that measurements done on unpassivated wafers cannot be used for efficiency estimates, while others claim that, though difficult, it is possible and that there is great potential in these kinds of measurements.

McHedlidze et al. report in an article from 2012 that without proper passivation of wafers the low intensity of BB-PL signals will not allow correct material characterization. The shadowing effect also influences any results. It is first when polished and passivated that BB-PL images can give an accurate map of carrier lifetime. They claim that the potential for PL images is as a tool for exploring recombination activity of different defects, for determining the effects of gettering mechanisms and for wafer- based defect engineering. The largest barriers to be overcome being surface recombination and optical shadowing from grain boundaries. [6]

Trupke et al. published an article in 2011 where they looked into PL images taken at room temperature of as-cut wafers. They used these for characterisation of wafer material and to find spatially resolved lifetime data. They conclude that: "only areas with severely reduced bulk lifetime will show up with significant contrast in spatially resolved effective lifetime data"[7], and these areas strongly correlate with the performance of the final cell. Even though surface recombination makes measurements challenging, there is a larger potential for saving resources when defective wafers are found in an early stage. [7]

Johnston et al. did studies published in two articles where they compared PL images of multicrystalline silicon wafers at room temperature at different process steps and compared them to finished cell performance. They found that some defect areas stay unchanged, while some change throughout the process. While realizing the difficulties of measuring unpassivated wafers due to surface recombination, they see that as-cut wafer classification is possible. For a summed area over a threshold value in the BB-PL images there is an evident correlation with open circuit voltage (Voc) and short circuit current (Isc). In their findings a percentage of a wafer covered by DRL signal correlates even better with final efficiency, Voc and Isc. They also found that the DRL image of the as-cut wafer correlated better with poor performance regions of the finished cell than the DRL images of ARC- processed wafers did. [8] [9]

3.2 Defect Related Luminescence (DRL) Lines

'D lines' refers to four different defect emission signals called D1, D2, D3 and D4 which have their respective energies. They are listed in Table 3.1. Although some authors mention other D lines, those are not considered here. D lines are believed to be caused by dislocations in crystalline material. [5] The D lines are often reported to appear in pairs: D1 with D2 and D3 with D4.

Arguirov et al. published an article on spatially resolved PL measurements at 80 – 300 K performed on ribbon-grown silicon samples. They report that although an inverse correlation between BB-PL and D1 emissions was expected, they observed correlation between D1 and BB intensity at grain boundaries and areas of increased surface recombination. In addition to this, their results confirm the theory that D3 is a replica of D4, and they observe an additional peak at energies close to D4, which at high temperatures cannot be spectrally resolved from D4. [10]

Binetti et al. published a review paper presenting results and developments of PL and infrared spectroscopies. However, only information regarding PL of non-dopant impurities and DRL is considered here. As some of the conclusions reported in the paper come from measurements done on sc-Si, Binetti et al. warn that care should be taken when PL analysis of mc-Si, solar grade Si or upgraded metallurgical Si is done, as these types of materials contain more defects. [11]

Binetti et al. mention in their review paper that D1 always appears as dark lines on the BB-PL mapping, is highly temperature stable, and is the only DRL signal visible at room temperature. The characteristics of both D1 and D2, like energy position and intensity are affected by the presence of different impurities. [11]

They further report that while carbon (C) is the main non-dopant impurity in solar grade mc-Si. Other common impurities are oxygen (O), nitrogen (N) and 3d transition metals (Fe, Ti, Mn, Cu). Carbon is a substitutional impurity, while oxygen and metals are generally interstitial impurities. Because of their characteristics, metals are usually investigated with

other means than PL, which leaves carbon, oxygen and nitrogen compounds as the most important for PL analysis. [11]

They report that while “oxygen and carbon agglomerates and complexes are involved in different PL centers.”[11] The different emission lines listed by Binetti et al. are included in Table 3.1. [11]

Flo et al. studied DRL on passivated mc-Si wafers over the height of an ingot at 80K and 300K. Different signals were separated by MCR analysis. They studied the four D lines, a line called VID3 and found 3 more signals, at approximately the same energies (0.68, 0.7 and 0.8 eV), which are potentially the same one. For the D lines they found that D1 and D2 are not always on the same place, while D3 and D4 are. VID3 is an emission line at 0.94 eV which is similar to D3, but with different characteristics. Flo et al. state that this emission pattern corresponds to other authors’ findings. The additional emission lines reported by Flo et al. are included in Table 3.1. [12]

3.3 Origin and Cause of DRL Signals

There have been identified additional DRL signals other than D lines. Most of them also have a theory of the most likely cause.

Mudryi et al. conducted among other things PL measurements with high spectral resolution of small samples (1 cm^2) of sc-Si and mc-Si, and compared these at different temperatures down to 4.2K. They examined the D-lines as well as 5 other lines called A, C, T, I and H lines. The T line (0.9355eV) and I line (0.9652eV) are believed to be caused by carbon and oxygen impurity atoms together with hydrogen. The A line (0.9697 eV) and C line (0.7894 eV) are believed to be caused by “the formation of carbon- and oxygen-related centers.”[13] They also found that the D-lines can be best seen at 78 K, and these are the strongest signals observed at this temperature. They further state that their measurements showed the energy position of the main D2-D4 lines and a 0.8 eV band to vary with ±5 and ±20meV respectively, and that the 0.8 eV band could be related to D1, but it has a slightly different spectral shape and energy position. [13]

Tajima et al. look at the D-lines and a 0.78 eV band, and the photoluminescence maps before and after Fe contamination. Their findings “support the idea that the D3/D4 lines are intrinsic to dislocations, and that dislocations are electrically activated by heavy metal contamination.”[14] They also conclude that the “0,78 eV band is associated with oxygen precipitation and has different origin from the D lines.” [14] In 2012 Tajima et al. report that D3 and D4 are intrinsic to dislocations, and are strong there, if not hindered by oxygen. [15]

3.4 Temperature Dependency

It is known that characteristics of different DRL signals are temperature dependent. The following is information from some articles exploring this temperature dependency.

Inoue et al. analysed the PL spectrum of an etched mc-Si wafer in the temperature range 15 - 300 K. They found that the position of measured peaks shifted and intensities changed. They found a broad signal at 0,78 eV at 300 K, which was at 0,82 eV at 150 K, and attributed the peak shift to the band gap shrinking. They conclude that this emission signal is a composed both D1 and a signal called Db. [16]

Schubert et al. explored DRL at temperatures between 80 and 300 K at points on a defect-rich mc-Si sample. They found that positions of peaks varied greatly across temperatures. They could not draw conclusions as to what causes these changing emission lines. They find a relatively stable emission line at 0.838 eV at a defect-rich area. [17]

Arguirov et al. performed among other things PL measurements at 12 different temperatures between 80 and 300 K, of passivated samples. They then deconvoluted emission signals into Gaussian peaks. They found that D1 and D2 are not of the same intensity, while D3 and D4 are approximately of the same intensity. They then compared the temperature dependency of peak intensity and width. They found that at different temperatures, D1 grows at the same rate as D3 and D4 diminish. [18]

Tajima et al. also explore signals at different temperatures, and they report of an additional signal at 0.87 eV which they do not detect at temperatures below 100 K. At approximately 100 K D1/D2 merge and D3/D4 merge into a common signal for each pair, and a new signal at 0.87 eV appears. This signal moves to lower energy regions with higher temperatures. [15].

3.5 Summary Table

Table 3.1 gives a summary of the different emission lines reported in some of the literature, with the D lines and BB-PL given in bold.

Name	Energy [eV] (Temperature)	Believed Cause
	0.68, 0.7 and 0.8	Unknown [12]
N1- N5	0.745 (4.2K) – 0.773 (4.2K)	Complexes involving N [11]
P line	0.767	Oxygen related donors [11]
C line	0.789	Complex involving C and O [11]; O-related centres [13]
D1	**0.807**	**Dislocations**
D_b	0.768(300K) – 0.820(77-150K)	Oxide precipitates [11]
(D1 and D_b)	0.78 (300K), 0.82 (150 K)	D1 and D_b combined [16]
-	0.838 (over 100 K)	Unknown [17]
D2	**0.870**	**Dislocations**
-	0.87	Not D2 [15]
H line	0.9255	Complex involving C and O [11] [13]
D3	**0.935**	**Dislocations**
T line	0.9355	C, O and H[13]
VID3	0.94	Unknown [12]
I line	0.9652	C, O and H [13]
G line	0.969	Zero-phonon emission line caused by C and N [11]
A line	0.9697	Carbon-related centres [13]
D4	**0.998**	**Dislocations**
BB	**1.12**	**Band to band emission [3]**
-	1.1223 (4,2K)	Complexes involving N [11]
Grain boundaries	Dark lines	Grain boundaries [11]

Table 3.1: Summary of some reported emission lines
D lines and BB-PL are shown in bold. The emission lines in the table are taken from [11], [13] , [12] , [17]and [16].

4 Experimental Setup and Data Processing

Section 4 presents the material examined in this thesis, experimental details, a presentation of the method used while performing the experiment and the method used for the analysis of the results.

4.1 The Wafer Samples

The wafer samples used in this experiment were provided by Hanwha Q CELLS GmbH. There were 17 sets of wafers with approximately 10 wafers in every set. Each set comes from the same ingot. The samples were produced by 5 different producers (which are confidential), and six of the sets were standard multicrystalline silicon while the remaining 11 sets were high performance multicrystalline (HPM) silicon wafers. HPM solar cells achieve better efficiency than standard multicrystalline solar cells through the use of crystal growth technology for defect control. [19]

The samples were full size wafers of 15.6 cm × 15.6 cm. The wafers have been cut, but neither etched nor coated, and are thus unpassivated.

Every wafer is identified by a unique name and number, etched onto the wafer's upper left corner. It is assumed that a higher number means it's taken from a position higher up on the ingot, as grain sizes clearly increase with a higher number.

We were provided with data for the neighbouring wafers' performance when finished as a cell.

To reduce the scope of this thesis only three of the sets are analysed. These are the "B2", "HM" and "A2+C" sets. None of these sets are from the same manufacturer, and "B2" is a set of standard wafers, while "HM" and "A2+C" are HPM wafers. These three sets were chosen because they show somewhat different emission patterns. The name and number for the 30 wafers analysed are listed in table 4.1. The remaining 5 sets are not yet analysed.

B2 set	HM set	A2+C set
B2_005	HM_005	A2+C_005
B2_011	HM_011	A2+C_011
B2_014	HM_017	A2+C_014
B2_023	HM_026	A2+C_029
B2_035	HM_038	A2+C_041
B2_053	HM_047	A2+C_056
B2_065	HM_053	A2+C_071
B2_074	HM_065	A2+C_086
B2_083	HM_086	A2+C_095
B2_092	HM_095	A2+C_104

Table 4.1: List of wafers analysed
An overview of the 30 wafers imaged and analysed in this thesis. The name of each one is printed on the upper left corner of the wafer. The wafers belong to three different ingots, each made by a different producer.

4.2 Equipment Description

The experiments for this master's thesis were conducted at the Norwegian University of Life Sciences (NMBU) during spring of 2014, and relied on equipment there.

4.2.1 Movable Rig

A figure of the equipment used in this experiment is shown in Figure 4 .1. The largest parts were the table and the movable rig. The rig with the camera and laser were controlled through a computer program provided by the manufacturer.

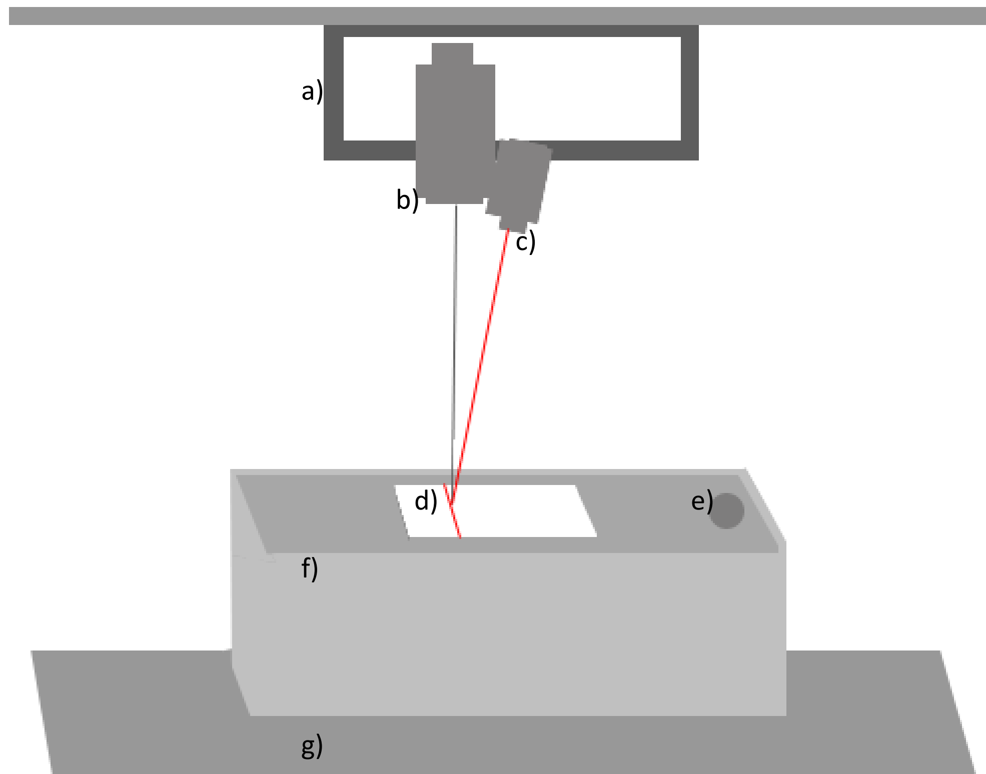

Figure 4.1: Equipment used in this experiment
a) moving rig, b) camera, c) laser, d) wafer sample, e) hole for pouring liquid nitrogen f) cryogenic cooler and g) table.

4.2.2 Cryogenic Cooler

The cryogenic cooler was constructed by Arne Svendsen, technician at IMT, NMBU. It is a steel container with an aluminium top, isolated by a layer of polystyrene.

On the top of the container there is a hole to add liquid nitrogen, which holds -196°C at atmospheric pressure. Once the container is cold, a wafer can be placed on the built-in aluminium surface top. The container is built in such a way that evaporated nitrogen is blown on the wafer sample, further cooling it down and helping avoid frost.

There are also two types of aluminium plates available. One type is used to place under the wafers, to help lift them up again. The other plate is used in place of the wafers. It has five screws on it where a temperature probe can be attached, allowing temperature to be measured. It is shown on Figure 4.2.

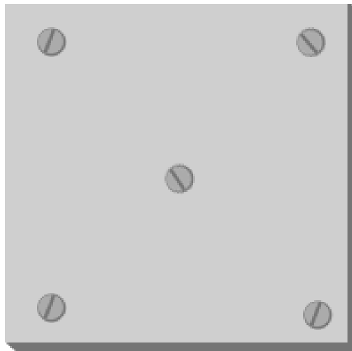

Figure 4.2: Aluminium plate used when finding temperature
This plate was placed on the cooler. The temperature was measured by attaching a temperature probe to the different screws.

Liquid nitrogen was used to cool the sample to approximately -180° Celsius, 90 Kelvin.

4.2.3 Laser

The laser used in this case is a Lasiris Magnum II (808 nm, 5W, Coherent Inc., Portland, USA). It is attached to the movable rig together with the camera in a distance of 33 cm from the measuring sample. The lasers' intensity is controllable. It is set to maximum on standard settings, giving intensity at the sample of approximately $3W/cm^2$.

4.2.4 Camera and Filter

The camera used for the hyperspectral imaging is an HgCdTe SWIR camera (Specim, Spectral Imaging Ltd, Oulu, Finland). It measures electromagnetic waves in the range 900-2500 nm, which corresponds to 0.49 eV – 1.34 eV. The camera records the signals from one row of pixels at a time. Incoming light is split through a prism into 256 bands of wavelengths. The intensity in every band is recorded before the camera moves to the next row of pixels. The interval for each band is varying, and is shown in Table 4.2. The spectral information is of high resolution; this is why it is called 'hyperspectral'.

In a certain setup the camera can measure 300 pixels over one 15.6 cm long sample, giving the images a spatial resolution of 2 pixels/mm.

The laser of 808 nm lies outside of the camera's detection limit. However, a high pass filter of 850 nm is used to prevent laser light entering the camera's detectors, as a second harmonics is in the detectable range.

The camera's settings are controlled through a computer program provided by the manufacturer, and include: frame rate, exposure time, scanning speed, retrace speed, scanning length, and duration of AutoDark. AutoDark is a section on the image where the

camera records for a few seconds with a closed shutter after scanning the sample. It is used to record pixel variation from the detectors.

Table 4.2: Centre energy of each band recorded by the camera [eV].
(Next page) The centre energy is listed for each of the 256 bands recorded by the camera in eV. A band refers to an energy range recorded by the camera with no spectral resolution. Band energies are listed downwards then left to right, and listed from band number 1 to band 256. This list is an adapted version of a list provided by the manufacturer.

1,338691	1,03516	0,844199	0,712983	0,61727	0,544366
1,329618	1,029735	0,840594	0,710417	0,615349	0,542876
1,320667	1,024366	0,837024	0,70787	0,613443	0,541394
1,311835	1,019062	0,833485	0,705345	0,611549	0,539923
1,303108	1,013804	0,829975	0,702834	0,609666	0,538458
1,294509	1,0086	0,82649	0,700341	0,607795	0,537
1,286023	1,003457	0,823039	0,697869	0,605933	0,535553
1,277648	0,998359	0,819616	0,695411	0,604085	0,534111
1,26938	0,993312	0,816222	0,69297	0,602248	0,532677
1,26122	0,988323	0,812857	0,69055	0,600422	0,531252
1,253163	0,983377	0,809518	0,688144	0,598608	0,529833
1,245209	0,978488	0,806207	0,685757	0,596804	0,528424
1,237355	0,973639	0,802923	0,683387	0,595011	0,527023
1,229599	0,968846	0,799666	0,68103	0,593229	0,525626
1,221941	0,9641	0,79644	0,678692	0,59146	0,524239
1,214388	0,959392	0,793235	0,676371	0,589699	0,522858
1,206917	0,954738	0,790055	0,674062	0,587948	0,521485
1,199537	0,950129	0,786901	0,671772	0,586208	0,52012
1,192247	0,945564	0,783773	0,669497	0,584478	0,518762
1,185057	0,941035	0,780673	0,667238	0,582761	0,517411
1,177941	0,936557	0,777594	0,664991	0,581052	0,516065
1,17091	0,932121	0,774543	0,662762	0,579355	0,514728
1,163974	0,927727	0,771511	0,660548	0,577665	0,513398
1,157109	0,923374	0,768503	0,658349	0,575985	0,512075
1,150334	0,919062	0,765524	0,656164	0,574317	0,510759
1,143628	0,91479	0,762562	0,653994	0,572657	0,509449
1,137011	0,910557	0,759628	0,651838	0,571008	0,508147
1,130459	0,906364	0,756716	0,649697	0,569369	0,50685
1,123992	0,902208	0,753822	0,647572	0,567737	0,505561
1,117599	0,898098	0,750955	0,645459	0,566117	0,50428
1,111268	0,894018	0,74811	0,643359	0,564506	0,503003
1,105019	0,889975	0,745281	0,641272	0,562902	0,501733
1,098839	0,885968	0,742478	0,639199	0,561309	0,500469
1,092728	0,882004	0,739696	0,637143	0,559725	0,499214
1,086685	0,878069	0,736935	0,635097	0,55815	0,497962
1,080708	0,874169	0,734195	0,633063	0,556584	0,496718
1,074787	0,870309	0,731474	0,631046	0,555027	0,495481
1,06894	0,866477	0,728774	0,629039	0,553479	0,494248
1,063156	0,862685	0,726094	0,627047	0,551939	0,493024
1,057434	0,85892	0,723433	0,625065	0,550407	0,491804
1,051774	0,855193	0,720792	0,623099	0,548884	0,490591
1,046183	0,851493	0,71817	0,621142	0,54737	
1,040642	0,847831	0,715567	0,6192	0,545864	

4.2.5 Computer Programs

Two computer programs were used for data collection and several more for data processing. The first computer program (Spectral DAQ, Specim, Version 6.62.181.24-R) was used to control the movement of the rig and the settings of the hyperspectral camera.

The second computer program, ENVI 5.0.1 Classic, was used to look at the imaging files before any processing was done. ENVI allows us to choose three bins of a certain wavelength to be shown in different colours, thus allowing us to have a preview of the imaging results. Due to a large amount of noise on the unprocessed images, it was occasionally hard to distinguish between signals and noise with the ENVI program.

In addition to these computer programs, MATLAB and Solo+MIA, Adobe Photoshop and Fiji ImageJ were used for data processing and presentation. This is explained in Section 4.4: Data Processing.

4.2.6 Other

A Canon camera was used to take RGB images of a selection of the wafers. For this, even lighting was also required.

4.3 Equipment Setup and Data Collection

The data collection for this master's thesis was done using the equipment described in Section 4.2. The following section describes how the experiment was conducted.

4.3.1 Cooling with Liquid Nitrogen

Liquid nitrogen evaporates at 77 K. Both liquid nitrogen and nitrogen gas can be harmful so it is important to take necessary precautions like using heat isolating gloves and safety goggles and doing the experiment in a well-ventilated room.

Liquid nitrogen was poured frequently into the cryogenic cooler for approximately an hour before it reached its minimum temperature, which was a surface temperature of 94 K ± 4 K at the surface with no lid on.

4.3.1.1 Recording Temperature

To be able to measure the temperature of the wafers, the ends of the sensor for an electric thermometer were attached to five successive points on the aluminium plate shown in Figure 4.2. Temperatures ranging from 90 K to 99 K have been measured, but different points showed approximately the same temperature (±1 K) within short time or during low activity around the wafer.

Fluctuations in temperature are believed to be caused by changes in the amount of liquid nitrogen in the cooler and activity on and around the cooler, like changing metal plates or wafers, or changing the position of the temperature probe.

It is not believed that a range of ± 4 K has a significant impact on our results. However, there is potential for improvement in the temperature stability of the experiment. Other uncertainties, which are also believed to be insignificant, are the thermometer's uncertainty and the temperature rise due to heating by the laser.

4.3.2 Moving the Wafers

The wafers are fragile and crisp when cooled. The aluminium plate to place underneath was crucial to avoid breaking them when getting the wafers out of their position on the cooler. Directly using gloved hands to move the wafers was found to be safer than using tweezers as this gives a better feel of how much strength is being used. When off the cooler the wafers tended to either stick together or float around depending on the amount of air between them.

A good rule seemed to be to avoid lifting more than ten wafers (one set) at a time. Unaligned, the weight of a few sets of wafers seems to be enough to break one.

For consistency all wafers were laid under the camera with the same orientation, with the name appearing on the top left corner on the images. Some sets of wafers were slightly bigger than the others. For some this was solved by letting them cool for one minute; for others the area to lay wafers on top of the cooler had to be expanded.

4.3.3 Operating Laser and Camera

The recorded images used in this thesis were obtained on March 12th and 13th 2014.

Before doing the measurements the camera's lens was focused to the distance of this setup and the laser aligned to the camera's line of view. Both focusing the camera and aligning the laser was more important for the final quality of the images and inexact calibration caused a first set of image files to become less than ideal. These images were later retaken.

Special safety glasses were used when exposed to the laser light.

Using software provided by Specim, settings were chosen. Frame rate was fixed to 25 Hz. Exposure time was set to maximum allowed on the software, which was 20 ms. With this exposure time, signal was detected. Scanning length was set to 200.00 mm to cover the whole wafer. Scanning speed was set to 13.00 mm/s, so that together with the rate of imaging, the resulting image had the original proportions. This way there was no overlap in the scanned pixel rows. AutoDark was set to 3 seconds.

The image file of one scan is approximately 74 MB before any processing, and takes approximately 18 seconds to take, not including preparations.

4.3.4 Additional Images

RGB images of a few of the wafers were taken using a Cannon camera for reference. A small sample of the wafers was also imaged with the hyperspectral camera at room temperature.

4.4 Data Processing

As mentioned earlier, several computer programs were used to analyse data. Following is a description of how this was done.

4.4.1 MATLAB

The raw files contain a large amount of systematic noise and measurement error from the camera. A basic clean-up is performed by subtracting signal in the AutoDark part from the rest of the file. The MATLAB code for doing this was provided by the research group. Next, the files were cropped to remove edges of the image, so that only the image of the wafer remained.

Based on what is described in the literature study, the image of emissions with selected energies were extracted and saved as Tagged Image Files (TIF). MATLAB was also used to check the spectrum at individual points.

4.4.2 Solo+MIA 7.5.2

Solo+MIA is a toolbox for MATLAB by Eigenvector Research, Inc., which can be used for hyperspectral image analysis.

Multivariate Curve Resolution (MCR) analysis was used for the statistical analysis of the hyperspectral images. MCR resembles Principal Component Analysis (PCA). It extracts information in the hyperspectral images as a number of components which contain significant signals. [12]

In this case the MCR was used to determine the different signals that exist on the wafer. The predetermined number of components was set to maximum (which was 20). Even though the number of components was set to 20, the program returned a variable amount of components: from 12 up to 20. Some of these components represented noise in the form of a line on the image where a sensor temporarily failed, or an area on the wafer where the laser was of uneven intensity.

Having chosen to look for 20 components on the MCR, the analysis could take up to one hour. This high number was chosen because the recorded noise is often so strong that it will be included as a component for in the MCR results before some of the interesting signals. When choosing fewer components signals were sometimes lost, and it was determined that simply removing components showing noise was a better alternative. It is important to remember that by choosing the maximum amount of components there might be some signals that are incorrectly divided into separate components.

An alternative would be to diminish noise on the images, for example by doing a mean of three images of the same wafer.

4.4.3 Adobe Photoshop CS5 and Fiji ImageJ 1.48a

Adobe Photoshop was used for the representation of some results, like overlaying MCR results and RGB images. Adobe Photoshop was also used to visualize the energy positions of peaks on the loadings curves found by doing the MCR analysis. These figures were drawn by hand and are therefore for reference only. More exact values can be found in the corresponding tables.

Fiji ImageJ was used to automatically label and position images in a montage of 256 different images.

5 Results and Discussion

As it is not possible to include detailed information on every wafer analysed, Section 5.1 presents detailed results and discussion for one wafer, namely wafer B2_053. Then, in Section 5.2 results and discussion for a whole set are presented and in Section 5.3 three sets are compared. Section 5.4 presents results and discussion of room temperature hyperspectral images and RGB images.

The 30 wafers examined for this thesis are listed in Table 4.1.

It is assumed that a higher number in the wafer name points to a higher origin on the ingot. This is based on the fact that sets clearly showed smaller grain size for wafers with low numbers and larger grain size for wafers with higher numbers. Images of the first and last wafer in the B2 set are included in the Appendix as Figure 0.1 and Figure 0.2. These wafers show a large difference in grain size.

5.1 Detailed Results for Wafer B2_053 at 90K

The B2_053 wafer is one of the middle wafers in the B2 set. It is chosen as an example because it shows many of the emissions typical for many of the wafers. However, no wafers show exactly the same results, and many wafers show both fewer and less intense emission signals than B2_053. Two methods were used to decide which wavelengths are important for this thesis. One is information in the Literature Study and the other MCR Analysis.

5.1.1 Analysis of Emissions by Using MATLAB to Extract Images

Each wafer was cooled to about 90 K and imaged in the range 900 – 2500 nm, which corresponds to 0.49 – 1.34 eV, using a hyperspectral camera. The resulting files were first pre-processed using MATLAB.

Each of the files can be seen as 265 images of the same wafer, each one taken at a different range of wavelengths or energies, called bands. To show this, a montage of the 265 images of each separate band for wafer B2_053 was made using Fiji ImageJ and shown in Figure 5.1. The centre energy of each band is listed in Table 4.2. Using MATLAB the images for each band can be written to a file separately, averaged, added or subtracted.

As can be seen from Figure 5.1, signals vary across the wafer and across bands. However, many of the images from single bands are similar. It would be neither correct nor efficient to try to analyse each band image by itself.

The first three rows of Figure 5.1 show no clear emission signal except noise. The fourth and fifth rows of Figure 5.1 are brighter than the rest. The bands at these energies correspond to the BB-PL signal from Si. The BB-PL covers large areas on the wafer. Most of row 5 and 6 appear black again, before at the end of row six an emission signal starts to appear and persist until the middle of row 9. This signal also covers large areas of the wafer, though less than the BB-PL. In row 10 and 11 there is an emission signal which is stronger at one

particular point on the upper right part of the wafer. In rows 12 and 13 there are more point-like emission signals spread out on the wafer. In the first half of row 14 the images of the wafer show an additional emission signal of almost uniformly bright large areas. Rows 15-20 show point-like emissions which become fewer and less intense on bands with lower energies. Rows after these contain mainly noise, with noise becoming stronger towards the low-energy bands. Noise is expected to become more pronounced towards the low-energy bands as the camera has less sensitivity in this area.

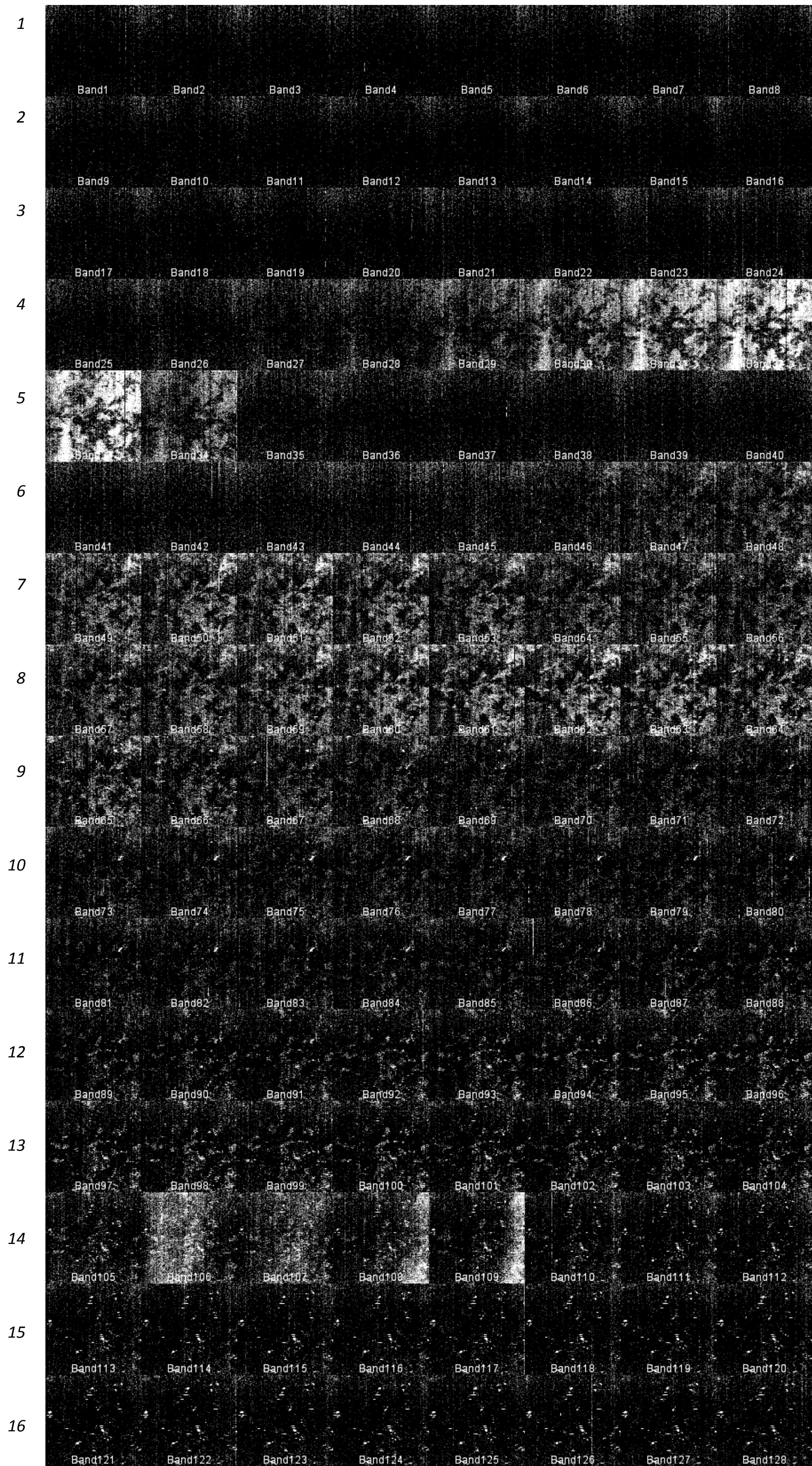
1
2
3
4
5
6
7
8
9
10
11
12
13
14
15
16
Band1
Band2
Band3
Band4
Band5
Band6
Band7
Band8
Band9
Band10
Band11
Band12
Band13
Band14
Band15
Band16
Band17
Band18
Band19
Band20
Band21
Band22
Band23
Band24
Band25
Band26
Band27
Band28
Band29
Band35
Band36
Band37
Band38
Band39
Band40
Band41
Band42
Band43
Band44
Band45
Band46
Band47
Band48
Band49
Band53
Band55
Band56
Band67
Band68
Band69
Band70
Band71
Band72
Band73
Band74
Band75
Band76
Band77
Band78
Band79
Band80
Band81
Band82
Band83
Band84
Band85
Band86
Band87
Band88
Band89
Band90
Band91
Band92
Band93
Band94
Band95
Band96
Band97
Band98
Band99
Band100
Band101
Band102
Band103
Band104
Band105
Band109
Band110
Band111
Band112
Band113
Band114
Band115
Band116
Band117
Band118
Band119
Band120
Band121
Band122
Band123
Band124
Band125
Band126
Band127
Band128

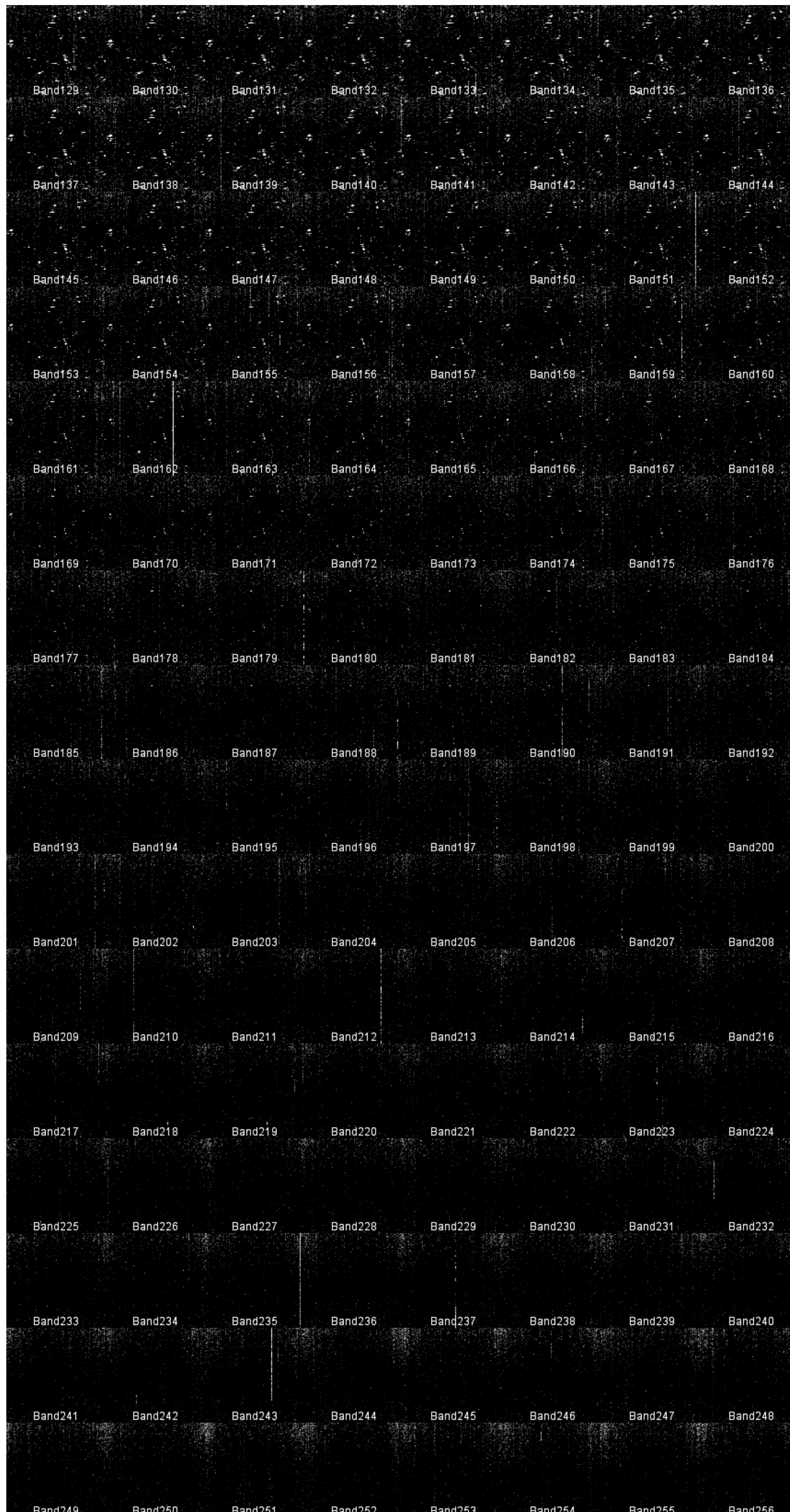

17

18

Figure 5.1: Montage of each separate band for wafer B2_053. *(Two pages) Each of the 265 images was taken simultaneously at different wavelength intervals. The centre energy of each band image is shown in Table 4.2. Each square is an image of the whole wafer with approximately 300 pixels in each direction. Black areas are areas on the wafer where no signal is recorded, and a lighter area means more emission is detected in this region at this wavelength. The montage shows rising band number from left to right.*

Based on previous studies (see Chapter 3) the most common emission signals are the BB-PL image and the D lines with energies of 1.12 eV (BB), 1.00 eV (D4), 0.935 eV (D3), 0.870 eV (D2) and 0.807 eV (D1). The five band images covering these energies are extracted and shown in Figure 5.2 (a). In Figure 5.2 (b) images are made by averaging signals from bands in and close to the same energy. This way noise can be reduced. Some images becomes less bright when finding averages over several bands, as the average is found including bands which show less intense emission signals.

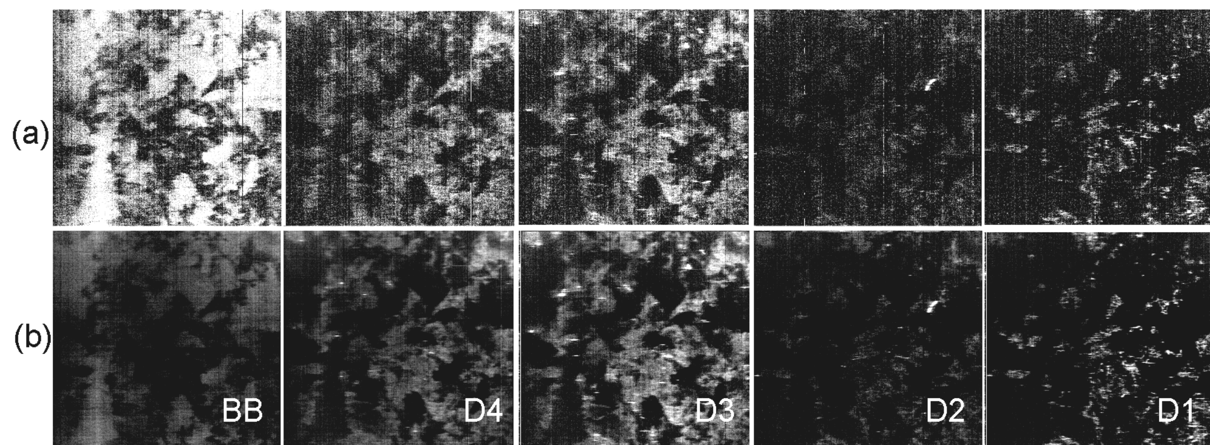

Figure 5.2: Five images of the B2_053 wafer at selected energies.
The images show emissions of energies of 1.12 eV (BB), 1.0 eV (D4), 0.935 eV (D3), 0.870 eV (D2) and 0.807 eV (D1). (a) shows images of a single band, while (b) shows images made by averaging the signals from 6 neighbouring bands, thus showing emission signals in the range of 1.143-1.051eV (BB), 1.046-0.950 eV (D4), 0.959-0.928 eV (D3), 0.882-0.859 eV (D2), 0.823-0.803 eV (D1).

From Figure 5.2 (a) it can be seen that BB-PL covers a large area of the wafer. D4 and D3 also cover large areas, but they are less bright. D3 and D4 are very similar, but in (b) it can be seen that the image for D3 has some bright points which D4 does not show. D2 and D1 are also similar, but while D1 is generally brighter than D2, D2 is bright only at one point. Comparing across the different emission signals we can see that the D lines seem to originate from approximately the same areas, which are mostly dark areas on the BB-PL image.

There are several other DRL signals at other energies being discussed in relevant literature. These are all potentially important and they are listed in Table 3.1. Figure 5.3 shows emission at three of these energies. The G line has energy of 0.97 eV, the H line of 0.93 eV and the N lines have energy of approximately 0.75 eV. The images for the G line and the H line show emissions which cover large areas. All three images show small bright points with different distributions on the wafer.

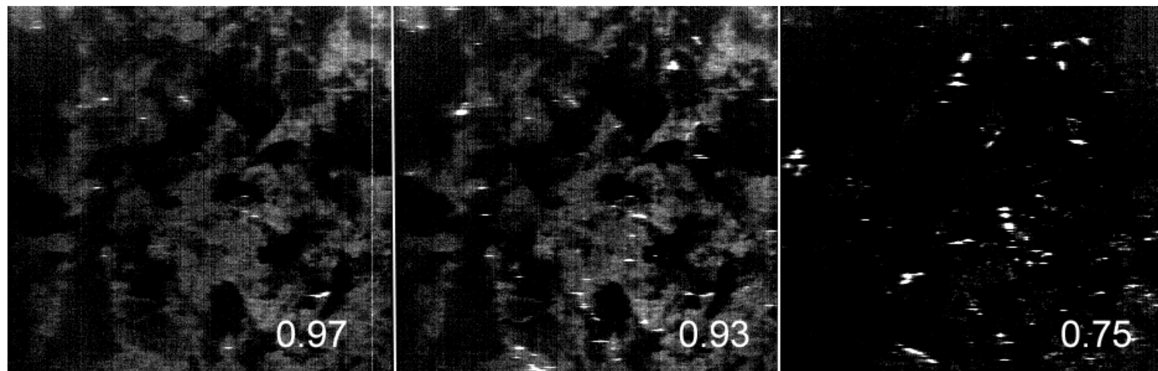

Figure 5.3: Detected emissions from wafer B2_053 with certain energies
The three images show emission with the energies of 0.97 eV (G line), 0.93 eV (H line) and 0.75 (N lines) eV. The first two images show similar large grey areas, but different small bright points. The image of emissions of 0.75 eV only shows bright points.

5.1.1.1 The 'VID3' signal

Based on an article by Flo et al.[12] and the work done by the research group working with this at NMBU, an additional image is extracted using MATLAB. With this we can explore the so-called VID3 signal. The VID3 signal shows up at approximately the same energy as D3, and they overlap. To distinguish it from D3 an assumption is made that the real signal from D3 and the signal from D4 extend over the same area and are very similar. The image of VID3 can thus be seen when subtracting the emission signal at energy of D4 (1.00 eV) from the signal at the energy of D3 and VID3 (0.870 eV). The resulting image is shown in Figure 5.4 (c). In Figure 5.4 (c) we see that because the image of D3 and D4 were not of the same intensity, a weak signal which is probably part of the D3 signal remains. VID3 shows up as bright points.

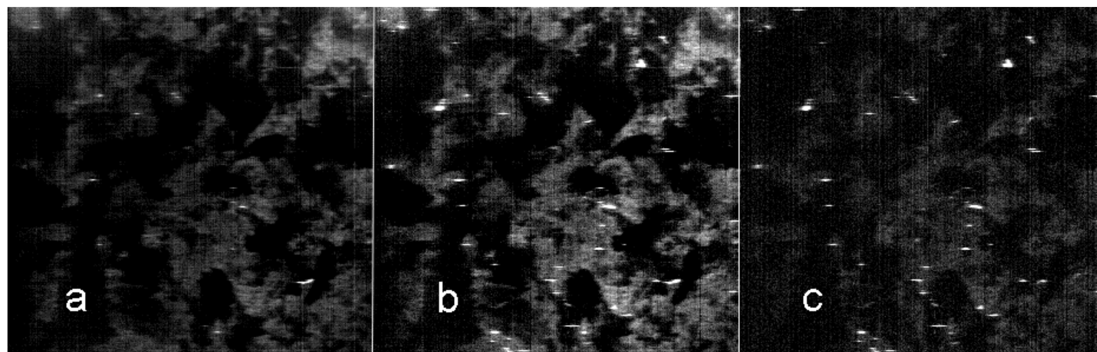

Figure 5.4: Finding VID3 for wafer B2_053 by subtraction
Images of wafer B2_053 of emissions at (a) 1.00 eV (D4) and (b) 0.935 eV (D3 and VID3). (c) is the resulting image found when subtracting image (a) from image (b). It is assumed to be the signal of VID3, which is point-like.

Figures 5.1 - 5.4 show that different positions of the wafer emit signals at different wavelengths. This means that different defects exist at different places. Areas that show a strong BB-PL and no DRL are ideal, while areas on the wafer which show no BB-PL are

defective areas. Some areas might show no emission, meaning that electrons in this area go through non-radiative recombination mechanisms.

If we look at separate images for all known emission signals, it becomes hard to see which images are different and which emission signals are present. Since many emission signals overlap, the fact that there are bright regions on an image does not mean a well-known signal at this energy is present in the sample. The MCR analysis done in this study is a better way to identify different signals.

5.1.2 MCR Analysis Results for wafer B2_053

In this section detailed results are presented for the MCR analysis of the hyperspectral image for wafer B2_053 at 90 K together with an analysis and discussion. To distinguish between different PL signals emitted by this wafer, the cropped and cleaned up image file containing all bands for the wafer was loaded into SOLO+MIA and an MCR analysis was performed with pre-processing of 'Multiway Center' and desired number of components set to 20.

Results were given in the SOLO+MIA program as a certain amount of components with a maximum of 20. For every component there is a map showing the distribution of this component on the wafer, called a scores image, and a graph showing its spectral distribution, called a loadings plot. The results for the MCR analysis of wafer B2_053 are 15 components with a cumulative fit of 41.57%.

In Figure 5.5 the scores image for the first component from the MCR analysis result for wafer B2_053 is presented. The colour code is given on the right, with light parts showing high emission, and dark parts showing less or no emission. While Figure 5.5 does resemble the image of emissions in the range 0.9 eV to 1.0 eV in Figure 5.2 and 5.3, it seems the bright points do not appear at the same positions as in any of those images.

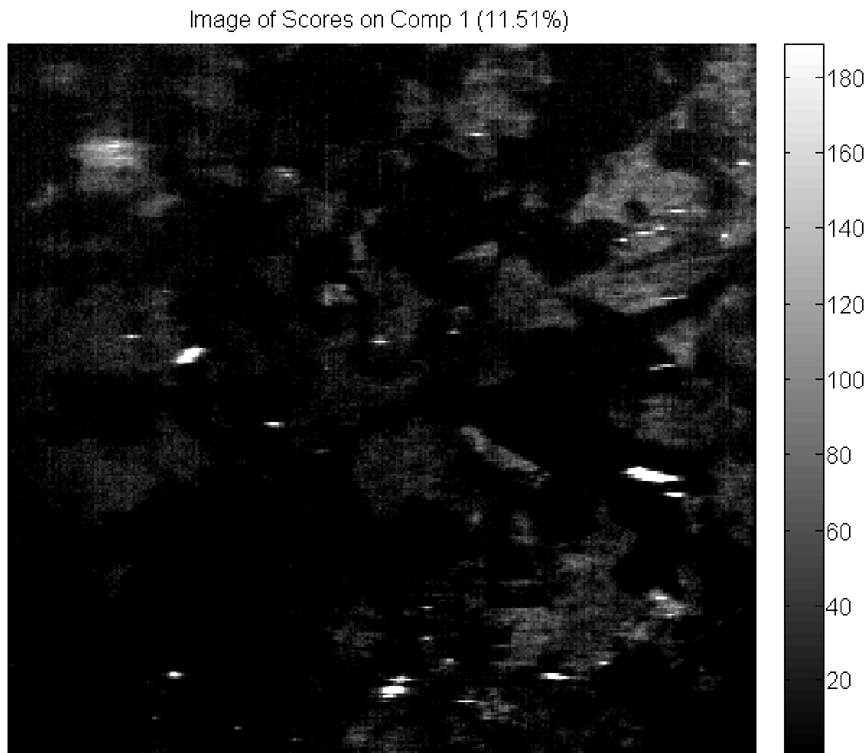

Figure 5.5: Scores image for component 1 from MCR analysis of wafer B2_053
The scores image for the first of 15 components obtained for this wafer. Values for the grey scale are shown on the right. The scale can be manually chosen, and corresponds to choosing the contrast of the image. A grey scale is chosen for this figure to make it comparable to Figures 5.2-4. Component 1 exists as some grey larger areas, and a few white points.

The loadings plot for the same component is shown in Figure 5.6. This plot indicates the bands at which this component appears. An energy scale is included at the top, showing that the peak of this component occurs at band 63 which has centre energy of 0.9410 eV. Although close to the energy of the D3 line and VID3, the scores image for this component was different than both these signals.

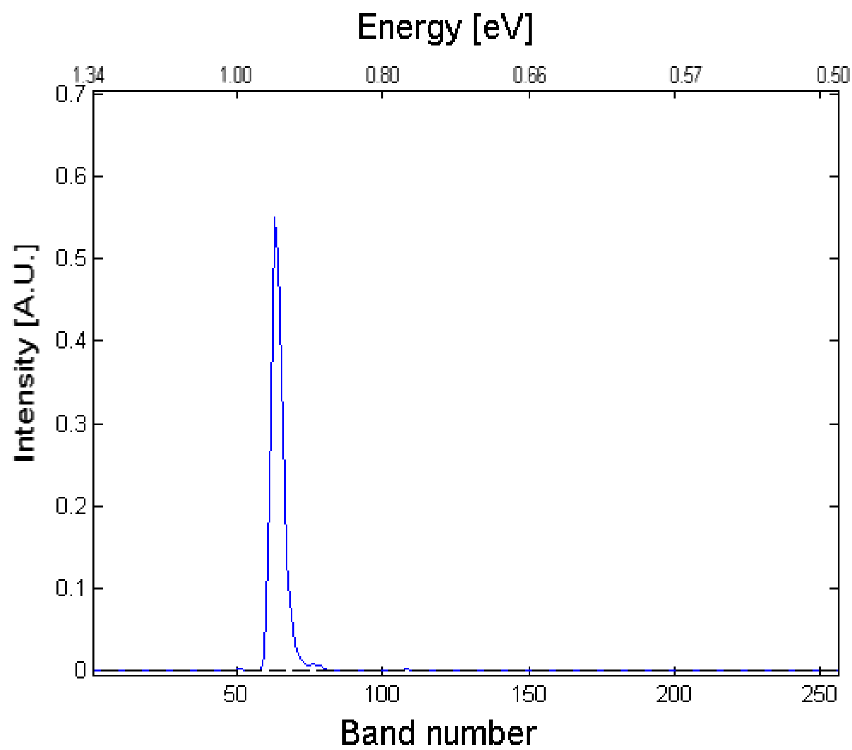

Figure 5.6: Loadings plot for component 1 from MCR analysis of wafer B2_053
The loadings plot for the first component obtained for wafer B2_053 is shown here in blue. The Y-axis shows intensity in arbitrary units, while the X-axis shows sinking energy and rising band number from left to right. The figure shows that component 1 has a peak at band 63 (0.94 eV), and stretches across approximately ten bands (0.05 eV).

In Figure 5.7 all the scores images of each of the components obtained through the MCR analysis of wafer B2_053 are presented. Component 5 and 12 are very similar and correlate with the image of BB-PL found in Figure 5.2.

Further in Figure 5.7 we can see that components 2, 4 and 14 are similar, and resemble the image for D3 and D4 in Figure 5.2. Components 1, 3, 6 and 7 show point-like signals, while components 8, 9, 10, 11, 13 and 15 are noise.

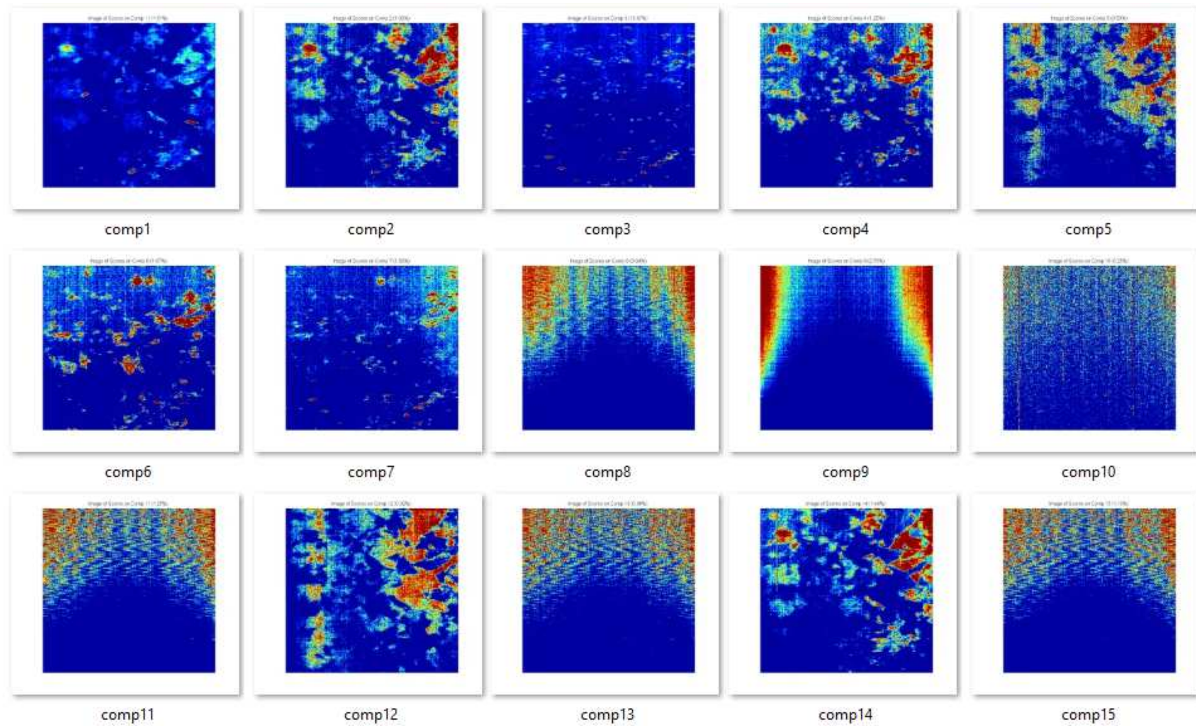

Figure 5.7: Scores images for each component from the MCR analysis result for wafer B2_053.
The 15 components are shown with a colour scale where red is a strong signal and dark blue is none. The contrast for these scores images is not common for the different components. Some of these components are similar, and some of the components are due to noise.

Larger images of components 8, 9 and 10 representing different types of noise are shown in more detail in Figure 0.5 in the Appendix. Components with scores images like these are caused by uneven illumination by the laser or faulty detectors in the camera. They are picked out as components by the MCR analysis because signal intensity is weak compared to noise intensity.

Components showing noise are identified and not further considered in this study.

When performing the MCR analysis, the desired number of components is always set to 20 , which is the maximum amount. This was done as restricting the number of components often resulted in significant signals being omitted rather than reducing the number of components showing noise.

Figure 5.8 shows a montage of the loadings plots for each of the 15 components obtained for wafer B2_053. From this we can also find out which components represent noise (components 8-11, 13 and 15), and link the rest with predetermined emission signals, like the ones listed in Table 3.1.

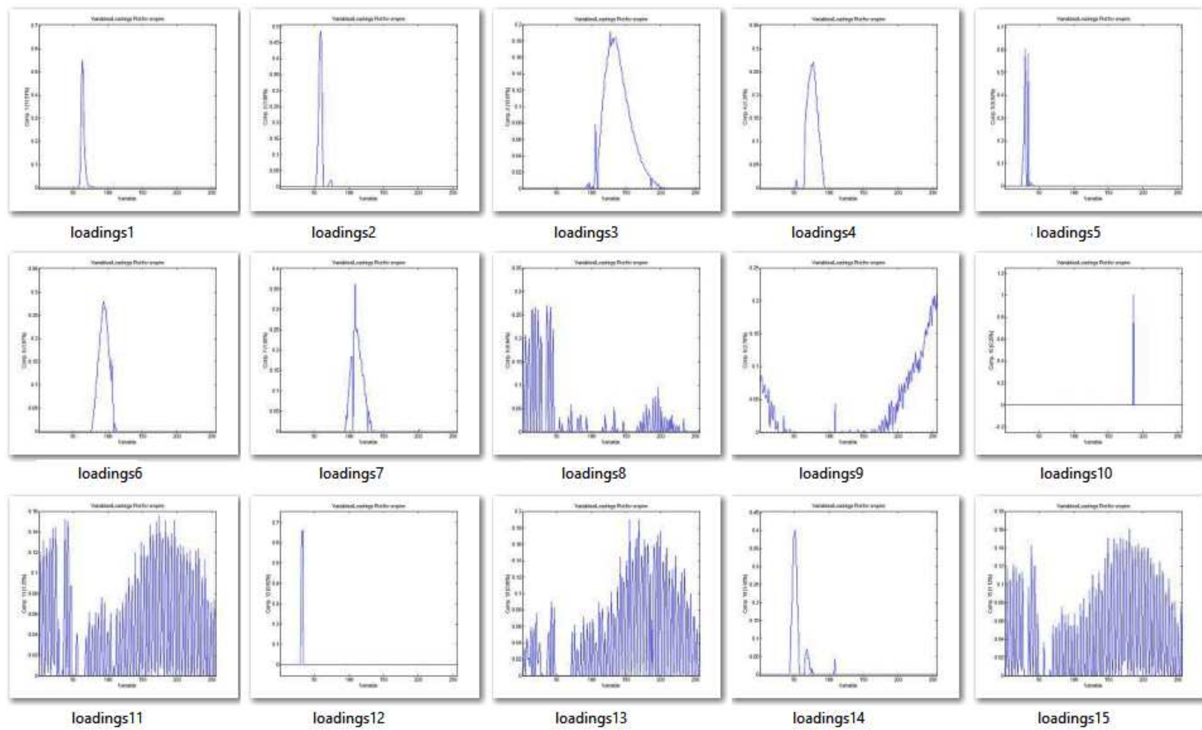

Figure 5.8: Loadings plots for separate MCR components for wafer B2_053.
The figure shows a montage of the loadings plots for the 15 components obtained by MCR analysis of wafer B2_053. They are not scaled with a common Y-axis for A.U. The X-axis of each plot stretches over the 265 bands taken by the camera. Components 8, 9, 10, 11, 13 and 15 show typical plots for components due to noise.

After extracting components showing noise, the remaining significant loadings plots can be plotted together for comparison. This is shown in Figure 5.9. Here it is easier to compare the energies at which different components peak. MCR analysis for this wafer resulted in 9 significant components where it seems two of them (components 5 and 12) represent the same signal (BB-PL).

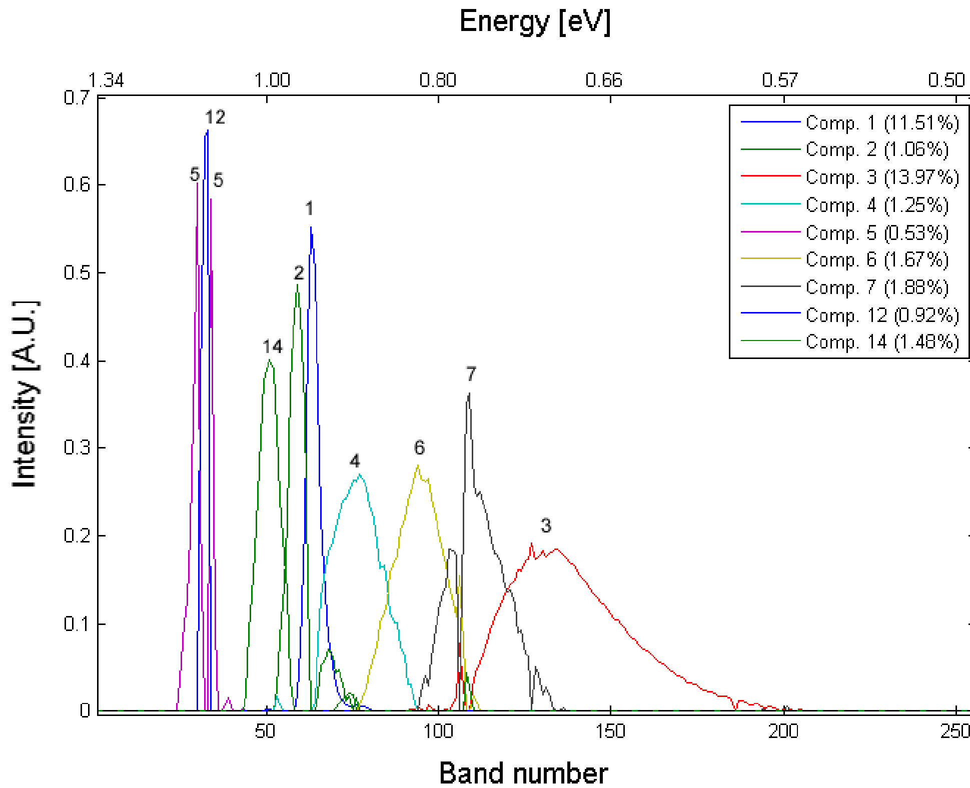

Figure 5.9: Loadings plot of significant components for wafer B2_053.
Nine components are included in this figure. Components showing noise are not included. Components to the left represent emission signals with a higher energy than those to the right. Two components (5 and 12) both have energies corresponding to BB-PL.

When examining Figure 5.9 we find that there are components with similar energies and shape. By comparing the score images for these components, we can determine whether they really represent separate signals. If they appear on different positions on the wafer, they are more likely to actually show different emission signals. Pairs which are compared based on similar peak energy are components number:

- 5 and 12
- 14 and 2
- 2 and 1
- 14 and 1
- 1 and 4
- 4 and 6
- 6 and 7
- 7 and 3

Other pairs, which are compared based on similar scores images are components number:

- 2 and 4
- 1 and 3
- 2 and 3

Each of these pairs is shown on the same image in Figures 0.6, 0.7 and 0.8 of the Appendix. One component is shown in red and the other in green, with areas common for both components shown in yellow. From these images it can be seen that the component pair showing the BB-PL signal blend into each other. Apart from these, all components are only partially present in the same positions. Those components covering the most similar area are components 2 and 14, shown in Figure 0.6-B, but even here there are areas which are only covered by one component. This suggests that except components 5 and 12 for the BB-PL, which seem to only be differentiated by an uneven emission across the wafer (possibly because of an uneven excitation source); all other components represent different emission signals.

In Figure 5.10 the combined loadings plot for the significant components obtained for wafer B2_053 are compared with some of the emission lines found in relevant literature. Some emission lines have a similar energy and partially overlap. The loadings plot of some components fit very well with the energies of emission lines from literature, while some have peak energies which do not correspond with the reported energies for emission lines. A closer inspection for each of the emission signals follows in Section 5.2.2.

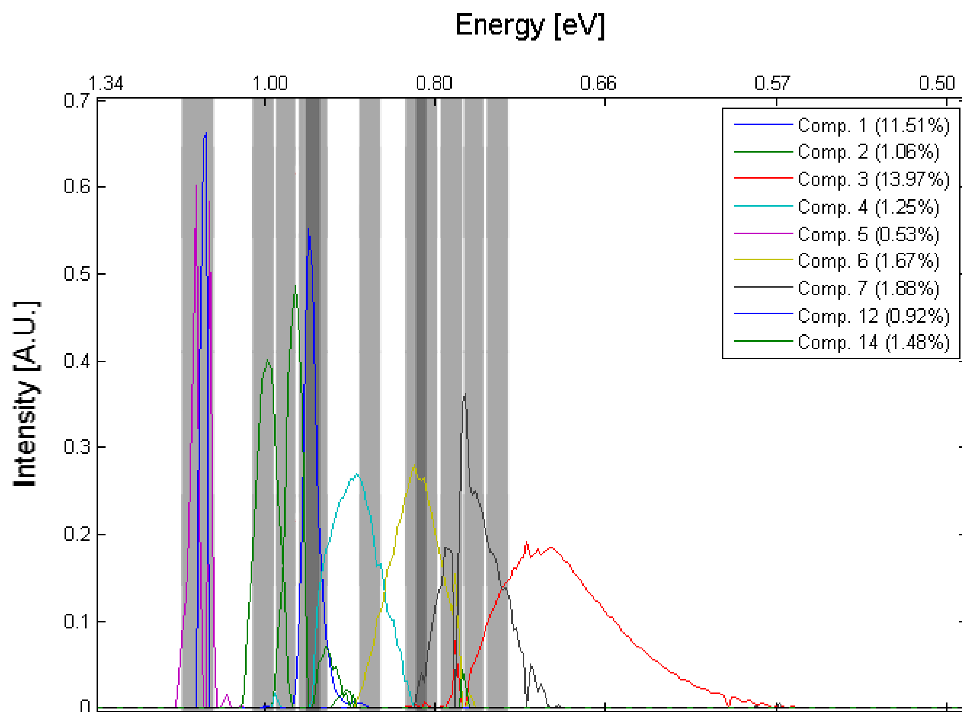

Figure 5.10: Components for wafer B2_053 and predetermined emission lines
A column has been inserted for some of the emission lines discussed in the literature study into the combined loadings plot for components obtained for wafer B2_053. It can be seen that some components correspond well with the predetermined emission lines, while others do not.

The same approach was taken when performing MCR analysis of the remaining wafers. It is important to remember that the obtained components with corresponding loadings plots and scores images are restricted by the effectiveness of the MCR analysis in extracting information from samples containing a large amount of noise.

5.2 Comparing Wafers from Different Heights in an Ingot

When comparing the results obtained for different wafers in a set we can examine differences that occur according to height of origin on the ingot. The results of this section are obtained through performing hyperspectral scans at 90 K.

5.2.1 Comparison of Emission Signals across the B2 Set of Wafers

In this section the results for the wafers in the B2 set are presented and discussed.

In Figure 5.11 six images of emissions at different energies, are shown for each wafer in the B2 set. This allows us to look at one signal at the time while comparing across the ingot.

It can be seen that the intensity of all the different signals generally increase with an increasing number (higher on the ingot). The contrast has been adjusted for the images of each wafer so that emission signals are visible. In the B2_005 wafer BB PL is barely visible, and the images for this wafer are of low contrast. We can also see that all of these images are affected by the grain size, with DRL for wafers with an origin low on the ingot all being point like, and the DRL for wafers with an origin high on the ingot all covering larger areas.

When comparing the acquired images for VID3 across wafers, one can see that towards the top of the ingot (wafer B2_092) the image for VID3 becomes less point-like, and more similar to D3 and D4. An explanation for this is if D3 and D4 are not of equal intensity. Then, simply subtracting the image at 1.000 eV from that of 0.935 eV does not correct for this difference in intensity, and parts of D3 will remain in the image for VID3. A more optimal image would be acquired through a method that corrects for intensity differences.

The BB-PL image for the different wafers is brighter in the lower left corner of the wafers. This might be a sign of uneven illumination by the laser.

While the images in Figure 5.11 are practical for examining emissions at predetermined energies, it is not appropriate when looking for other signals, and trying to determine how many emission signals are present.

Figure 5.11: Signals at selected energies for wafers in the B2 set

(Next page) Each row of images is of the same wafer at different energies. Each column of images shows one range of energies (an average of six bands). Energies shown are 1.1 eV (BB), 1.0 eV (D4), 0.935 eV (D3), difference between signals at 1.0 eV and 0.935 eV (VID3), 0.870 eV (D2) and 0.807 eV (D1). Images for different wafers are not of the same contrast

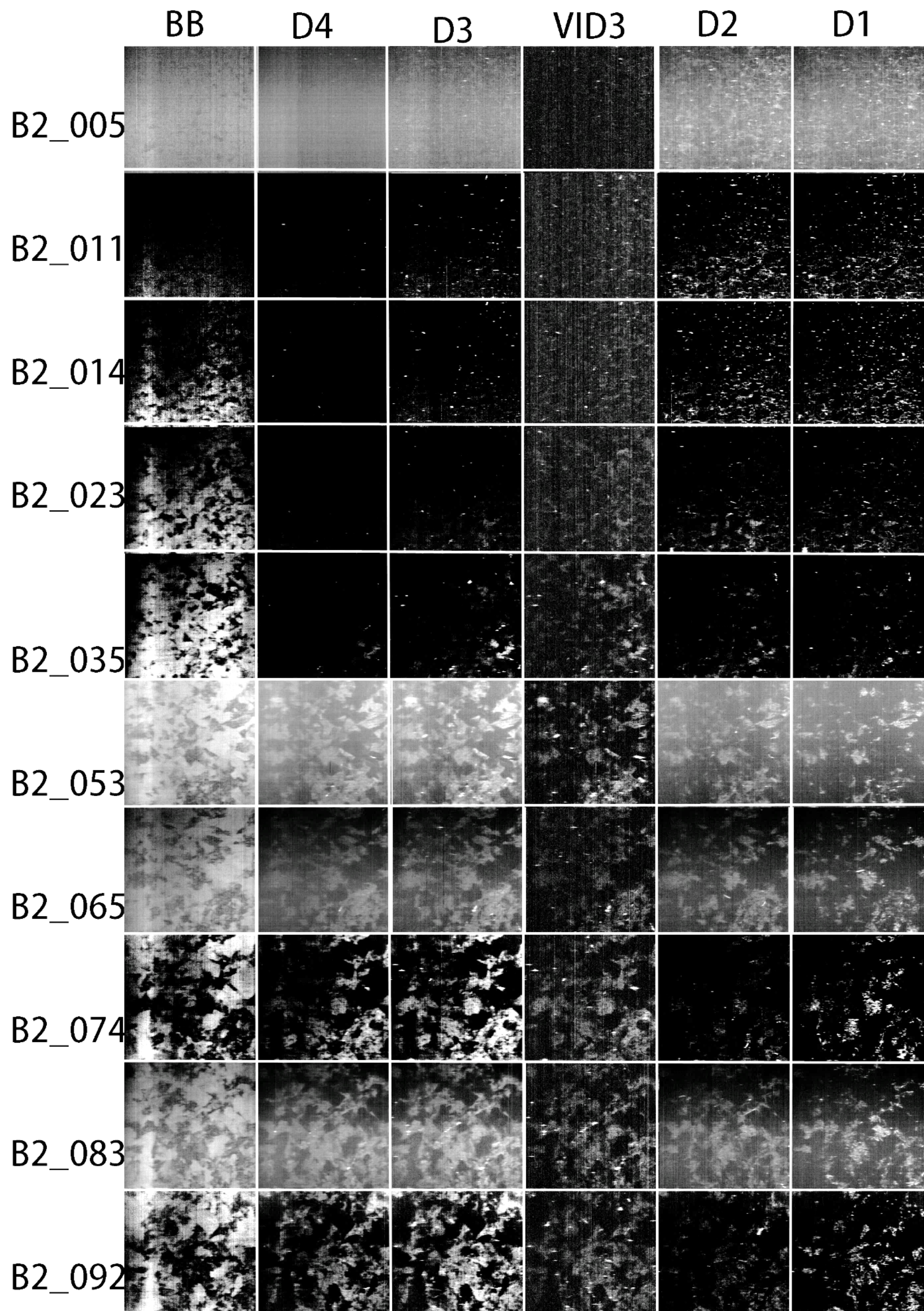
BB
D4
D3
VID3
D2
D1
B2_005
B2_011
B2_014
B2_023
B2_035
B2_053
B2_065
B2_074
B2_083
B2_092

5.2.2 Comparison of MCR Components across Wafers in the B2 Set

Even when components showing noise are included in the count, the MCR analysis for each wafer did not always result in the maximum amount of components. Figure 5.12 shows the amount of components obtained from the MCR analysis, and also the amount of significant components believed to be more than just measurement error. From this we can see that the number of significant components increases with a higher origin on the ingot.

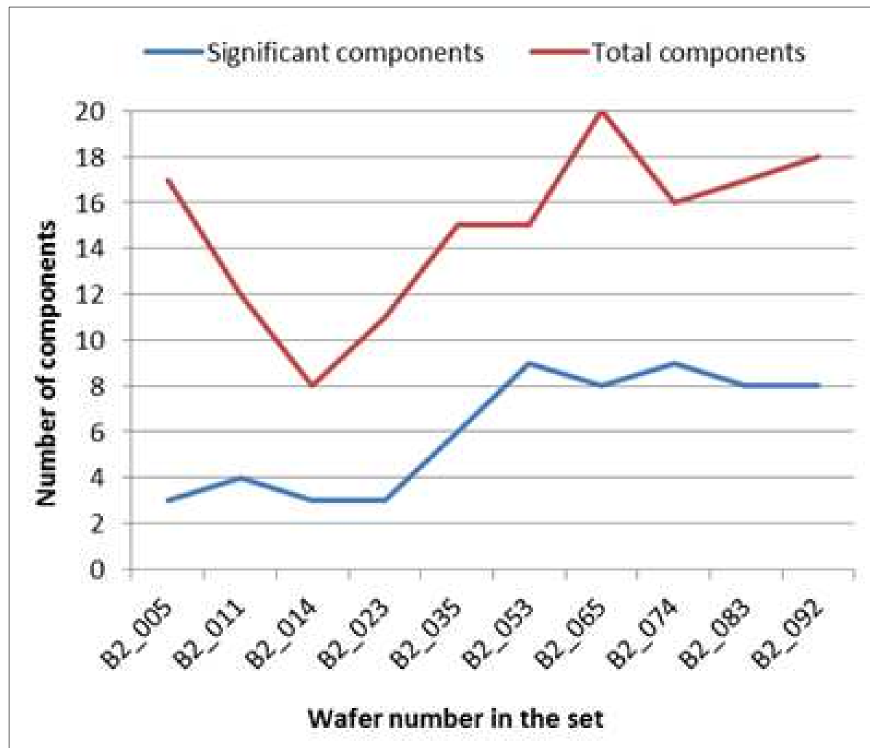

Figure 5.12: Number of components obtained for wafers in the B2 set
The maximum number of components obtained in the analysis is 20. The total number of components (red) varies greatly, while the number of significant components (blue) seems to be 3 or 4 for the four lowest wafers, and 8 or 9 for the 5 wafers highest on the ingot. The values in figure 5.12 are from the MCR result, and might be higher or lower than the real number of different signals emitted from the wafers.

Figure 5.13 shows an overview of the different components obtained in the MCR analysis for each of the wafers in the B2 set. Values at which loadings plots peak are shown as red dots, and predetermined important energies as grey columns. A red line connecting two red dots indicates that the loadings plot for this component had two peaks, while black lines connect components which are believed to show the same component. From this figure we can see that there is a correlation between many of the emission signals across wafers, and that there are more components for wafers from higher positions on the ingot. At the most it appears to be 8 different signals. We can also see that for the BB-PL and for the line of signals which starts at the position of D4, sometimes several points are connected and believed to be showing the same signal. For the BB-PL this is quite certain, while for the line of signals at D4 this is more unclear. We can also see that while some signals seem stable in

their peak energy positions, others are more variable, and there are alternative ways to connect these into one thread of signals. Thus, the lines connecting the dots are only a best guess. A closer analysis of each of the components follows.

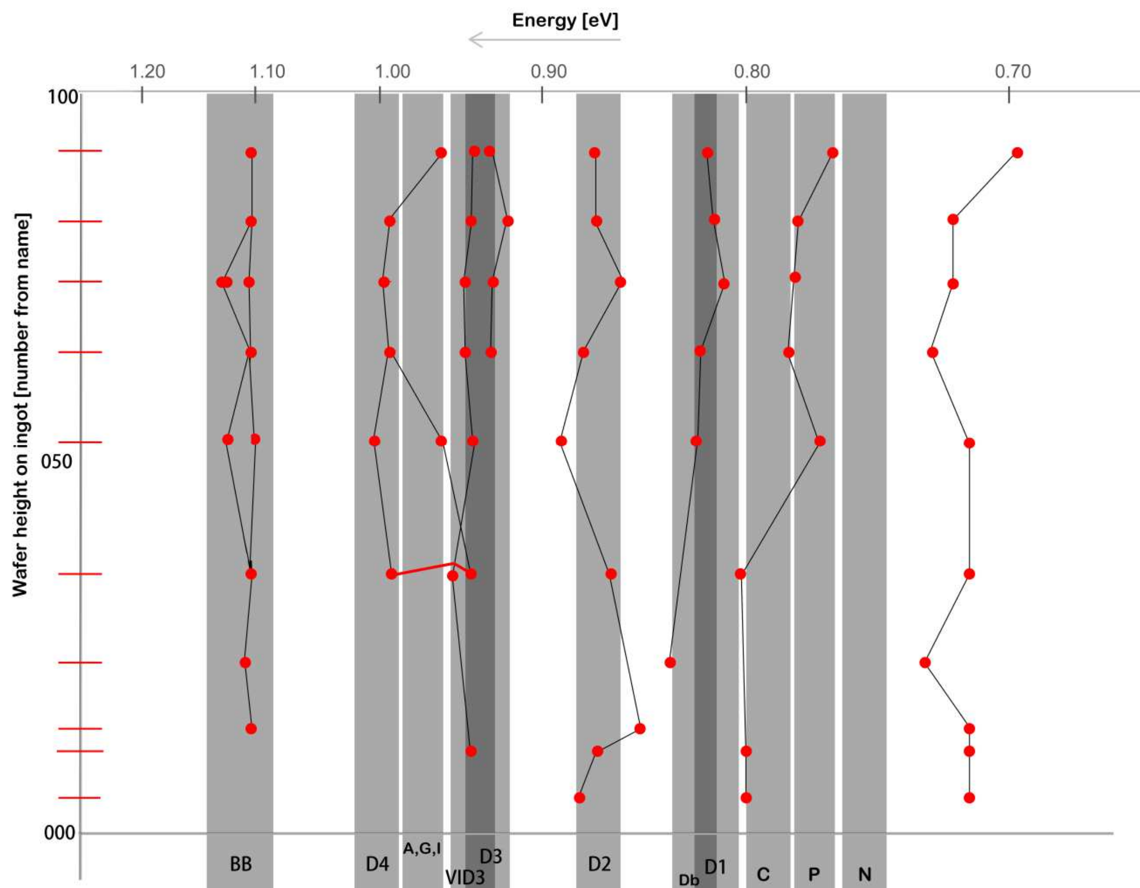

Figure 5.13: Peaks on loadings plots from MCR analysis results of B2 wafers
The Y-axis shows the number in the wafer name and position on the ingot rising towards the top, while the X-axis shows a rising band number from left to right, which corresponds to a sinking energy from left to right. Grey columns represent some of the predetermined important energies from the literature study. Each red dot is a top on a loadings plot of a component which is considered to be significant. A red line connecting two dots for wafer 035 means that this component has two tops. Black lines connecting the dots are a best guess for which components represent the same signal. The data points for this plot are attached in Table 0.1 of the Appendix.

In the rest of Section 5.2.2 the connected components in Figure 5.13 from different wafers which are assumed to be the same signal are plotted together for comparison, starting with the signal with highest energy, and continuing one by one. The colour code for these figures is shown in Figure 5.14, and applies to Figures 5.15-18, 5.20-21. The signals are compared to signals from literature, which are summarised in Table 3.1.

Figure 5.14: Colour code for figures showing signals from different wafers
Signals from each wafer are assigned a separate colour. The number corresponds to the number in the name of the wafer. The code applies for Figures 5.15-18, 5.20-21, and 5.23-24.

Figure 5.15 compares the components obtained for different wafers for energies at the position of BB-PL. From this figure we can see that the BB-PL signal is well defined and similar for all the wafers showing this component. It is narrow in its spectral range, with a base of about 20 bands (0.09 eV) for the main signal, and an extra shoulder on the low-energy side with intensity of approximately 1/20 with a range of 5 bands (0.03 eV). This signal is of high intensity, 0.5 – 0.7 A.U., for all the 8 wafers where this component was obtained. Two of the wafers in the B2 set did not show this signal. Moreover, we saw in the score image for wafer B2_053 (Figure 5.7, component 5 and 12) that a component at this energy extends over large areas and anti-correlated with other DRL emissions. We can therefore be certain that this component shows the BB-PL. Areas covered by this component will have better energy conversion efficiency as finished cells than areas not covered by it, as BB-PL is not related to defects. A high BB PL is also an indication that there are fewer non-radiative recombination mechanisms present in this area.

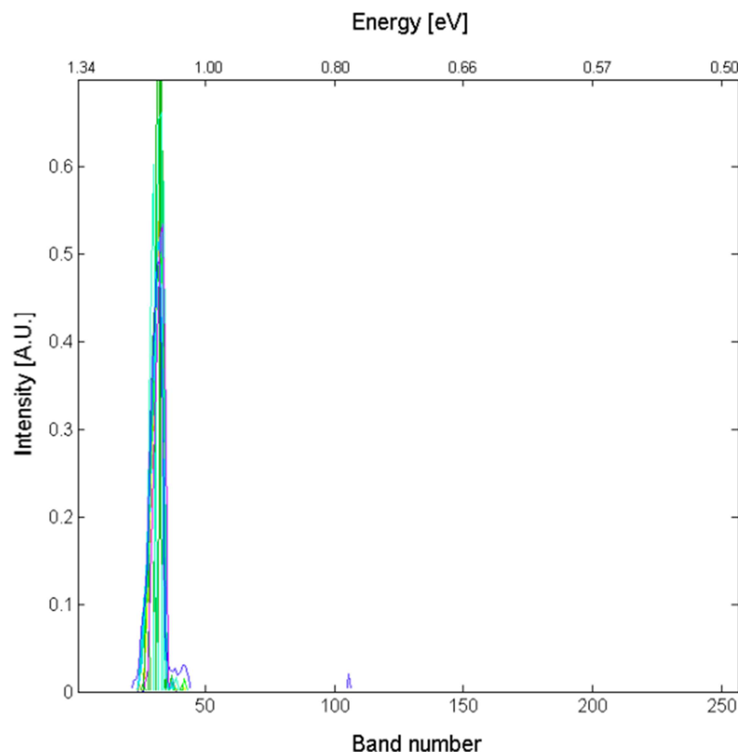

Figure 5.15: Loadings plots of components for B2-wafers, peak at bands 30-33
This signal shows up on 8 of the ten wafers, with two components (both inserted here) for wafer B2_053 and B2_074. The Y-axis shows intensity in arbitrary units, while the X-axis shows rising band number from left to right, which corresponds to sinking energy. Bands 30-33 have energies of 1.12 and 1.10 eV. This is the easiest signal to identify, as BB-PL is at 1.12 eV at room temperature and somewhat higher at 90 K. There are also no alternative signals close to this energy.

The next signal is shown in Figure 5.16. For this figure two components have been included for wafer B2_053. This component appears to contain three or four parts; one peak at band 50-52, one at 57-60 (wafers 035, 074, 083, 092), one at 69 (wafers 035, 053, 075 and 083) and one single peak at band 108 (wafer 035). This could be because the MCR analysis does not distinguish between the signals with these energies. For these wafers, several signals appear at the same places, so the MCR groups these into one component. There are no other components with peaks in the range of bands 57-60. The emission signal at wafer 108 is due to noise.

This signal is believed to contain at least two tops, one at band 52 and one at band 58. These correspond to energies of 0.99 eV and 0.96 eV. At these energies we have from literature D4 (0.998 eV), the A line (0.9697 eV), the G line (0.969 eV) and the I line (0.9652 eV). Although the I line is closest, the small difference makes it difficult to draw a conclusion. The components from the MCR results could also be a combination of several of these. D4 is expected to be in this sample, so this component is assumed to show D4 in its left peak with an additional signal as its highest peak at band 59. In Figure 0.6-B of the Appendix a

comparison is shown of the two components found for wafer B2_053 which peak at bands 52 and 59, and are both included here. It was established in Section 5.1.2 that these components are separate signals even though they cover similar areas.

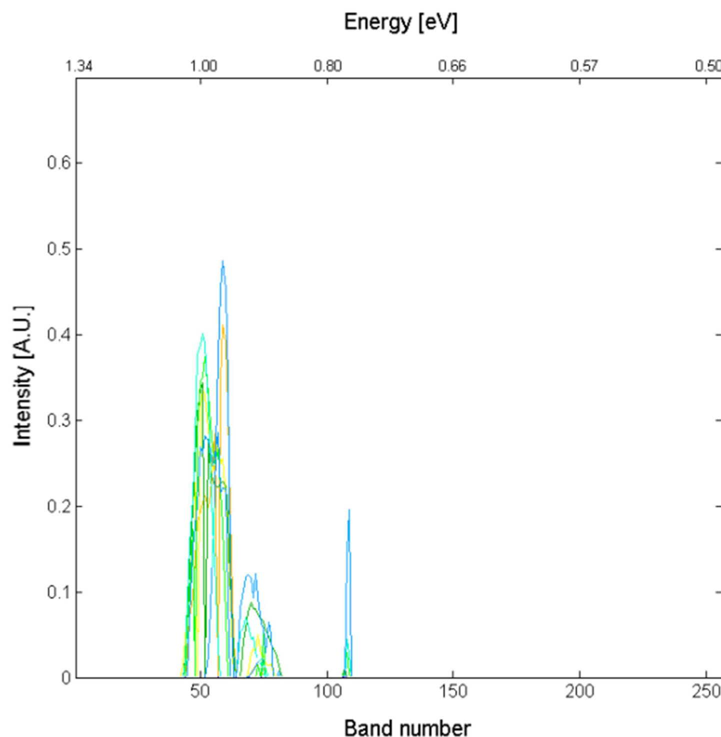

Figure 5.16: Loadings plots of components for B2 wafers, tall peaks at bands 50-52 and 58-59

This signal shows up on six of the ten wafers. (With two components for wafer B2_053: components 2 and 14) These components are the only ones in the range of bands 50-59, which correspond to energies of 1.00 – 0.96 eV. These are close to the D4 signal (0.998 eV) for the peak to the left and, the A line (0.9697 eV), the G line (0.969 eV) and the I line (0.9652 eV) for the tall peak to the right.

As before, the Y-axis shows intensity in arbitrary units, while the X-axis shows rising band number from left to right, which corresponds to sinking energy.

Figure 5.17 explores a narrow and intense signal which peaks at bands 62-63, (0.95 – 0.94 eV). Apart from the pink plot of wafer B2_011, 6 wafers show components with a maximum intensity of over 0.5 A.U.. The loadings plot of this signal is similar to the BB-PL signal in shape, with a spectral range of about 20 bands (0.09 eV) and an extra shoulder on either energy side, with intensity of less than 1/20 and a range of 5 bands (0.03 eV). This appears as a well-defined signal. When comparing Table 3.1 it is the VID3 (0.94 eV) signal that fits best. This signal has no recorded origin. Other close lines are the D3 line (0.935 eV), T line (0.9355 eV), I line (0.9652), G line (0.969 eV) and A line (0.9697 eV). From the scores image of wafer B2_053 which was included in Figure 5.7 as component 1, we see that this component strongest is point-like and does not cover larger areas. Although closest to the energy of

VID3, the scores image for wafer B2_053 does not resemble the image found when subtracting D4 from D3.

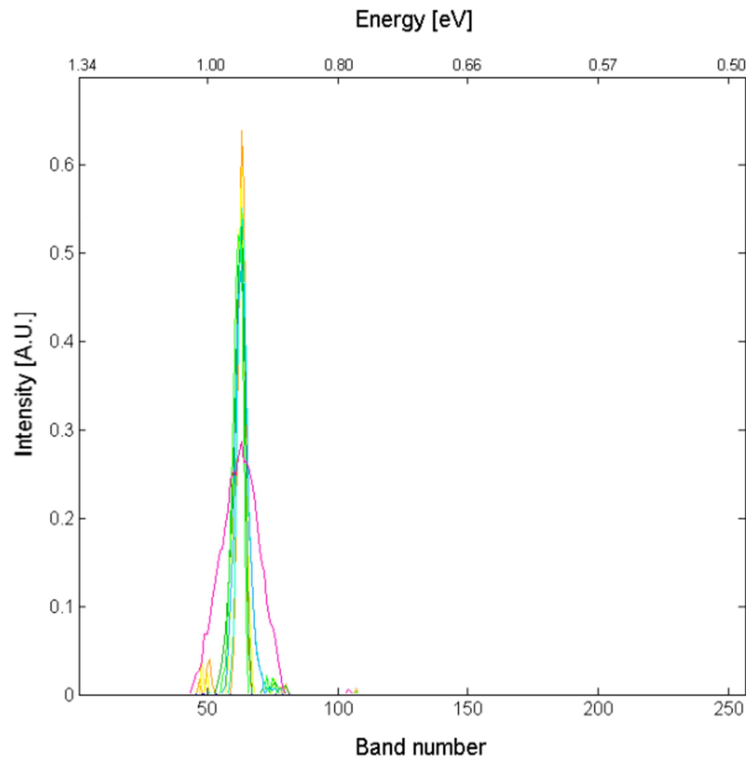

Figure 5.17: Loadings plots of components for B2 wafers, peak at bands 62-63
A component for the emission signal with a peak at this energy is obtained for seven of the ten wafers, with the signal of wafer B2_011 less intense and spectrally broader than the rest. Bands 62-63 correspond to energies of 0.95 – 0.94 eV. There are no known signals at this exact energy, and several possibilities in the neighbourhood. As before, the Y-axis shows intensity in arbitrary units, while the X-axis shows rising band number from left to right, which corresponds to sinking energy.

In Figure 5.18 a set of components similar to the previous ones are shown. These components are only obtained for four of the wafers in the B2 set. The loadings plots for the components from the four wafers are almost identical, with peak at bands 66-68 (0.93 – 0.92 eV), with a base for the main signal of approximately 10 bands (0.04 eV) and a shoulder for some of the components on either side of the signal with intensities of approximately 1/20 and widths of approximately 10 bands (0.04 eV). At the vicinity of the energy position of the peak of this loadings plot, we have the H line (0.9255 eV), D3 line (0.935 eV) and T line (0.9355).

For wafer B2_053 the scores image for this component was shown in Figure 5.7 as component 4. It is similar to component 14, which was determined to be D4. Since we know that D3 and D4 are usually reported to appear together, this suggests that the signal shown by these components is D3.

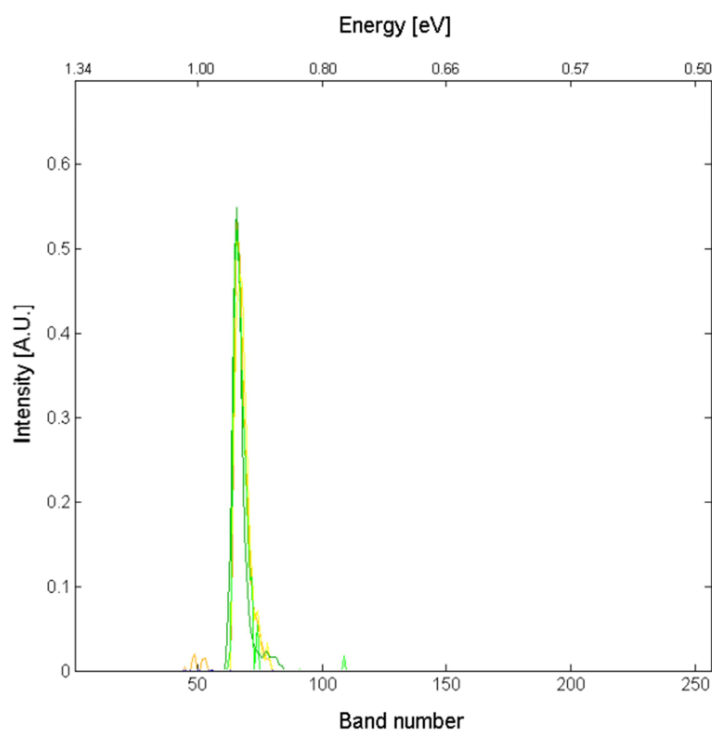

Figure 5.18: Loadings plots of components for B2 wafers, peak at bands 66-68
The figure shows signals from 4 wafers. This signal appears in the MCR analysis results for these four wafers as an additional component to the one shown in Figure 5.17. Bands 66-68 correspond to energies of 0.93 – 0.92 eV. This is close to the energy of the D3 signal, but there are also other signals with approximately the same energy. As before, the Y-axis shows intensity in arbitrary units, while the X-axis shows rising band number from left to right, which corresponds to sinking energy.

The plots in Figure 5.17 and 5.18 are similar, so a comparison of these is shown in Figure 5.19. The plots from Figure 5.17 with peaks at bands 62-63 (0.95 eV) are all plotted in orange here, and compared to those of Figure 5.18 for bands 66-68 (0.93 eV) in blue. We can see that there is a difference in their positions, and we can be more certain that these indeed different signals and not falsely separated in the MCR analysis.

This conclusion is also made based on the scores images showing both component types, such as the one shown in Figure 0.6-C of the Appendix, which shows that these two components cover different areas for wafer B2_053, and barely overlap.

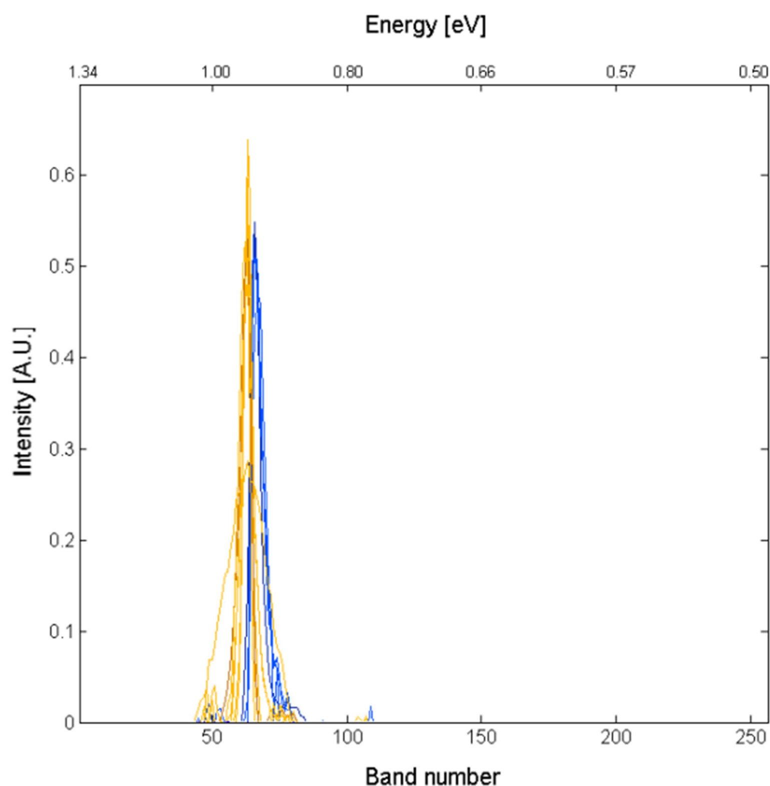

Figure 5.19: Comparison of components at bands 62-63 with those at bands 66-68
The two different components are probably two different signals. Components with peaks at bands 62-63 are shown in orange, and components with peaks at bands 66-68 are shown in blue. An orange component was obtained for seven wafers and a blue for four of those.
As before, the Y-axis shows intensity in arbitrary units, while the X-axis shows rising band number from left to right, which corresponds to sinking energy.

Figure 5.20 shows a signal which was obtained for 9 of the wafers (all except B2_023.) It was similar for 8 of them, but different for wafer B2_014, in that the component for B2_014 was spectrally much broader and of lower intensity. For the 8 similar wafers, the spectral range was 0.20 eV, while for B2_014 it was 0.29 eV. The maximum intensity for the 8 similar wafers

was between 0.2 and 0.3 A.U., while for B2_014 it was 0.18 eV. At the energy position of the peak of this loadings plot (0.86eV-0.89 eV) we know only of the D2 line at 0.870 eV. Wafer B2_092 shows a second peak at 1.00 eV. The reason for this is unknown. Plots of components with peaks at band 50 belong in Figure 5.16 (D4).

For wafer B2_053 the scores image for the component shown in Figure 5.20 appeared in Figure 5.7 as component 6, and showed point-like features.

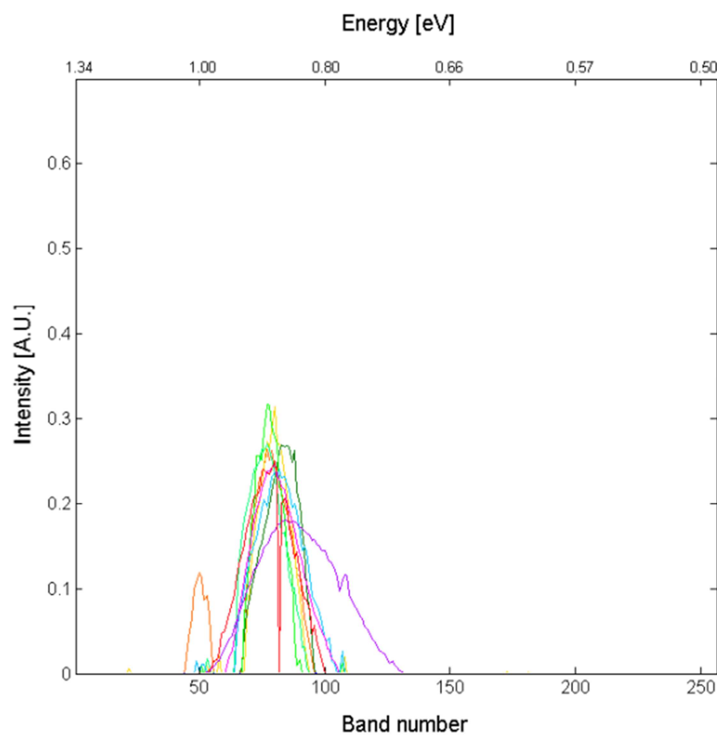

Figure 5.20: Loadings plot of components for B2 wafers, peak at bands 76-84
This signal shows up on 9 of the ten wafers. Bands 76-84 correspond to energies of 0.89 eV – 0.86 eV. This corresponds well with the D2 line at 0.87 eV. The purple plot belongs to wafer B2_014 and is much broader than the other component plots. The orange plot belongs to wafer B2_ 092 and shows a second peak at the high-energy side of the signal.
As before, the Y-axis shows intensity in arbitrary units, while the X-axis shows rising band number from left to right, which corresponds to sinking energy.

Figure 5.21 shows a component which was obtained for 6 wafers. For 5 wafers the signal is similar, while for one of the wafers, wafer B2_035, the loadings plot is spectrally wider and the maximum intensity lower. The five similar components plots belong to wafers B2_053 and up, and they all show this signal in addition to the signal believed to be D2. The peak energy of these plots changes slightly on the different wafers, and have a spectral range of approximately 0.15 eV. The division between the main part of the plot and the small curve on the low-energy side of the plot is believed to be caused by a component due to reflection at band 107-109, which is regarded as noise. The B2_035 wafer has a spectral range of 0.27

eV. The energy position of the peak of this loadings plot (0.81 eV-0.83 eV) fits perfectly with the combination of the D1 line at 0.807 eV and the D_b line at 0.820 eV reported by Inoue et al.. As the D1 signal is very common in the literature, this component is believed to contain the D1 signal, and not show the D_b signal only.

For wafer B2_053 this component (number 7) was strong at certain points and did not cover a large area.

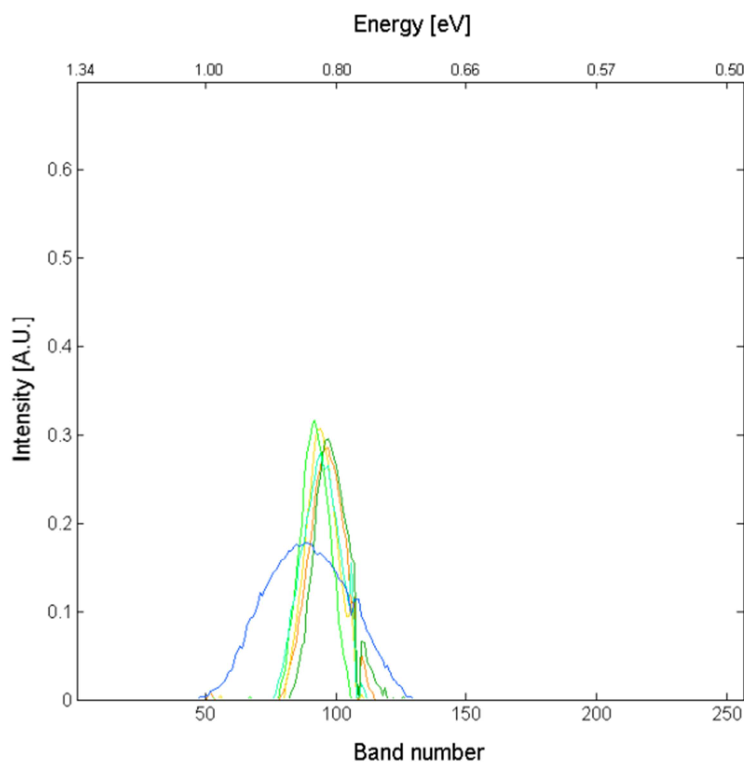

Figure 5.21: Loadings plot of components for B2 wafers, peak at bands 90-97
This emission signal shows up on six of the ten wafers. Five of the plots are similar and belong to the five uppermost wafers. The blue signal belongs to wafer B2_023 and is spectrally broader and has lower intensity than the others. Bands 90-97 correspond to energies of 0.83 – 0.81 eV. These components are believed to show the D1 signal.
As before, the Y-axis shows intensity in arbitrary units, while the X-axis shows rising band number from left to right, which corresponds to sinking energy.

Figure 6.22 shows a comparison of the components which are believed to be D1 and D2, shown in Figures 5.20 and 5.21. In this figure we can see that the two plots which were different from the rest in Figures 5.20 and 5.21, belonging to wafer B2_ 014 (orange) and B2_023 (blue) are very similar. They are of lower intensity than the other signals, and have a spectral range that is slightly more than the range of the D1 and D2 signals combined. It is therefore believed that for these two wafers D1 and D2 are so similar that the MCR analysis did not separate these into different components.

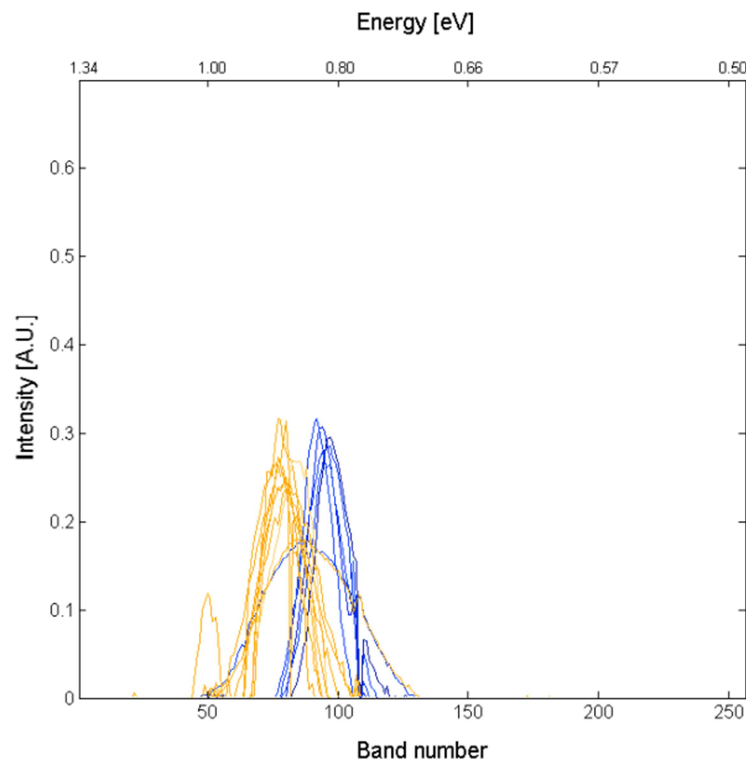

Figure 5.22: Comparison of components at bands 76-84 with those at bands 90-97
Loadings plots from Figure 5.20 which are believed to be D2 are plotted in orange, and plots from Figure 5.21, which are believed to be D1, are plotted in blue. The two broad signals belong to wafers B2_014 and B2_023 which only show one signal in total at this energy range. They spectral range of the two wide signals includes the range of both the orange and blue narrow signals. The narrow signal in blue is only obtained for the five wafers with highest positions on the ingot.
As before, the Y-axis shows intensity in arbitrary units, while the X-axis shows rising band number from left to right, which corresponds to sinking energy.

Two additional sets of components were explored. The first of these is shown in Figure 5.23. This is the most uncertain grouping of components for different wafers. This component is obtained for eight of the ten wafers. The most striking feature is the narrow and intense peaks shown by wafers B2_074 and, with less intensity, by B2_053. They appear at band 109 and are believed to be caused by reflection or a second harmonics to the laser. This is occasionally seen in the results for many of the other wafers, and is treated as noise. It is never broader than two or three bands. In this case, the MCR results include this noise as part of the component for this signal. Even though easy to identify, this reflection disturbs the MCR analysis, and could influence our results in and around this energy position. Giesecke et al. discuss ways in which correct for reflections. [20] We could try removing this signal by changing the filter to a better quality one, or by changing the angle between the laser and the camera.

The peak of the different components shifts slightly to lower energies with rising ingot height. The first three wafers that show this signal are B2_005, B2_011 and B2_035. The spectral range for these three is broader, and their peak is at a higher energy position. None of these three wafers showed a component the D1 signal, so the component in Figure 5.23 might be shifted to the left if the signal for D1 is included here. The spectral range for the first three wafers is 0.20 eV while the spectral range for the four narrower components is 0.14 eV. The peak of the first three wafers is at 0.80 eV while the peak of the remaining wafers is at 0.77 eV. Since the first tree wafers might contain an additional signal, the value for the remaining wafers is believed to be more correct for a signal at this position. From literature we know of the N lines at 0.745 – 0.773 eV (at 4.2K), the P line at 0.767 eV and the C line at 0.789 eV. Although it can be any of these, or even something else, the N lines and the P line are closest to the peaks of narrow signals.

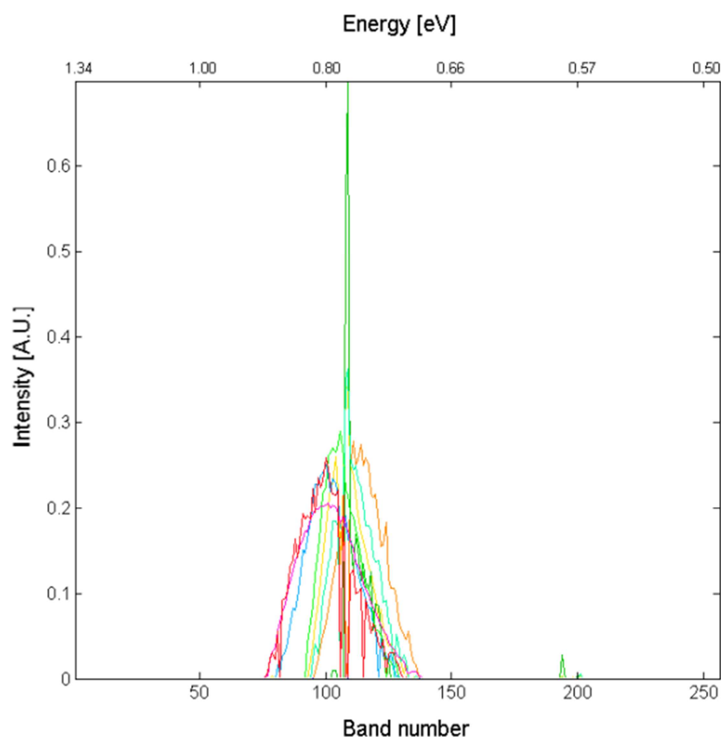

Figure 5.23: Loadings plot of components for B2 wafers, peak at bands 100-110.
This signal shows up on 8 of the ten wafers. They peak at slightly different energies, in the range 0.77 – 0.80 eV. Wafer B2_074 shows a narrow peak with strong intensity, Wafer B2_053 shows a less intense, but similar peak. This looks like a broad signal, but the width of the bands increases with increasing number. The spectral range of the signals lies between 0.14 eV and 0.20 eV. The plots peak at bands 100-110 which correspond to energies of 0.80 – 0.77 eV. There are three possibilities for matching signals in the literature, with the N lines (0.745 – 0.773 eV at 4.2K) and the P line (0.767 eV) being the most probable.
As before, the Y-axis shows intensity in arbitrary units, while the X-axis shows rising band number from left to right, which corresponds to sinking energy.

The component with the lowest energy position appears on all ten wafers, and is similar for all wafers. It is shown in Figure 5.24. All plots peak in the range 0.71 – 0.74 eV. As it is the only component obtained for all the wafers, it is clearly important. However, the only reference found to an emission signal with a similar energy is in Flo et al.[12], and no theories are found on the cause of this emission signal. The spectral range of the component is 0.26 eV, making it the spectrally widest component. The intensity is about 0.2 A.U. for all wafers.

The large amount of downward peaks on the plots is caused by components showing noise. There are more components showing noise in this energy range than in the range of other signals.

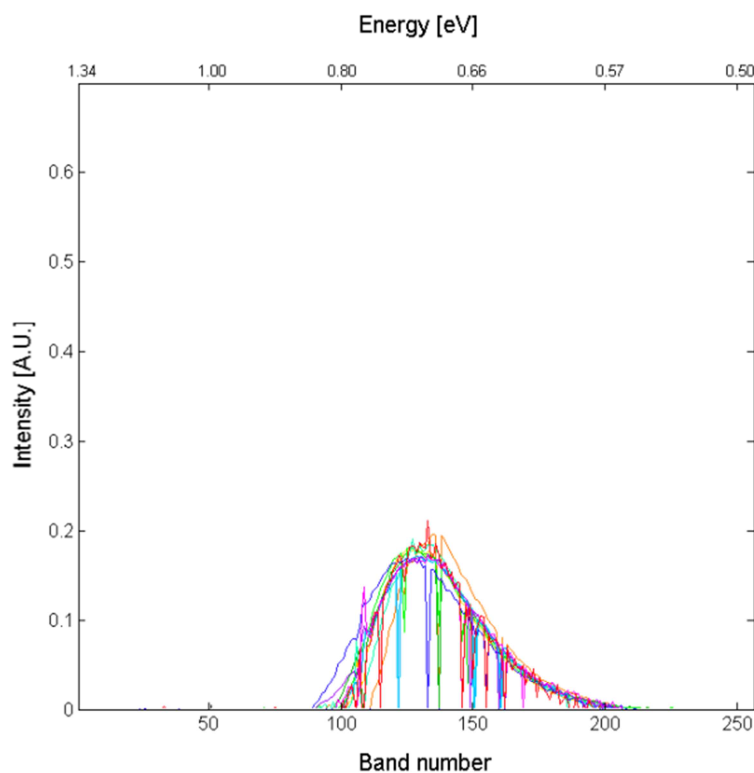

Figure 5.24: Loadings plot of components for B2 wafers, peak at bands 120-130
This is the only signal that is obtained for all of the ten wafers in the B2 set. It stretches over a large spectral area (0.26 eV). Bands 120-130 correspond to energies of 0.74 – 0.71 eV. The closest known emission signal in literature are the ones at 0.68 eV, 0.7 eV and 0.8 eV reported by Flo et al.
As before, the Y-axis shows intensity in arbitrary units, while the X-axis shows rising band number from left to right, which corresponds to sinking energy.

5.2.2.1 *Summary of Results from MCR Analysis of B2 Wafers*

Wafers with fewer components often show loadings plots with a broader spectral range, indicating several signals have been included into the same component.

Comparing components obtained for several wafers in a set make the distinction between different emission signals more certain, as similar results for different wafers help verify the distinction between different signals.

The different emission signals found in the B2 set are summarised in Figure 5.25. Eight different emission signals were identified, where one was the BB-PL and the other were defect related emission signals. Green squares represent components which are believed to be correctly differentiated. Yellow squares show components which are believed to be included in a resulting component, but which did not result in separate components. Black squares show signals which were not present in any components, and grey squares are highly uncertain.

Energy [eV]	1.11	1.00 + 0.96	0.94	0.92	0.87	0.82	0.77	0.72
Emission	BB	D4 + A/G/I	VID3?	D3	D2	D1+D_b	N/P	?
Band of peak	32	50 + 59	63	67	80	95	110	125
B2_005								
B2_011								
B2_014								
B2_023								
B2_035								
B2_053								
B2_065								
B2_074								
B2_083								
B2_092								

Figure 5.25: Summary of emission signals identified in B2 wafers
In this figure the energy for different signals is given at the top. For every wafer in the set these signals were either found as a separate component (green), included in a common component (yellow), not included in any component (black) or uncertain (grey).

Of the values for energies of different signals in Table 3.1 all the D- lines are believed detected in this sample, as well as some signals with energies corresponding to A/G/I line, VID3, D_b line and N/P line. In addition to these, one signal with a peak at 0.72 eV was obtained for all wafers.

As there are many factors influencing the results, the identification of some emission signals was not possible. There are also many signals mentioned in Table 3.1 which are not detected

at all. This is not unexpected, since some of the measurements mentioned in Binetti's article [11] were found in material which was processed through different methods.

5.2.3 Comparison of MCR Components across Wafers in the A2+C and HM Sets

In Figure 5.26 the peaks of components obtained for wafers in the A2+C set are plotted for comparison. As can be seen in the figure, a large number of components was obtained for all wafers in this set. There are some groups of components that have very stable energies across wafers, like the components with energies corresponding to D4, two signals in the VID3 region, one in D1 and one in P/N region. The total number of distinguishable emission signals is in the range 8 to 11. A further study is needed of the scores images of different wafers. Results indicate that some emission signals, particularily the BB- PL signal, is falsely divided into too many components.

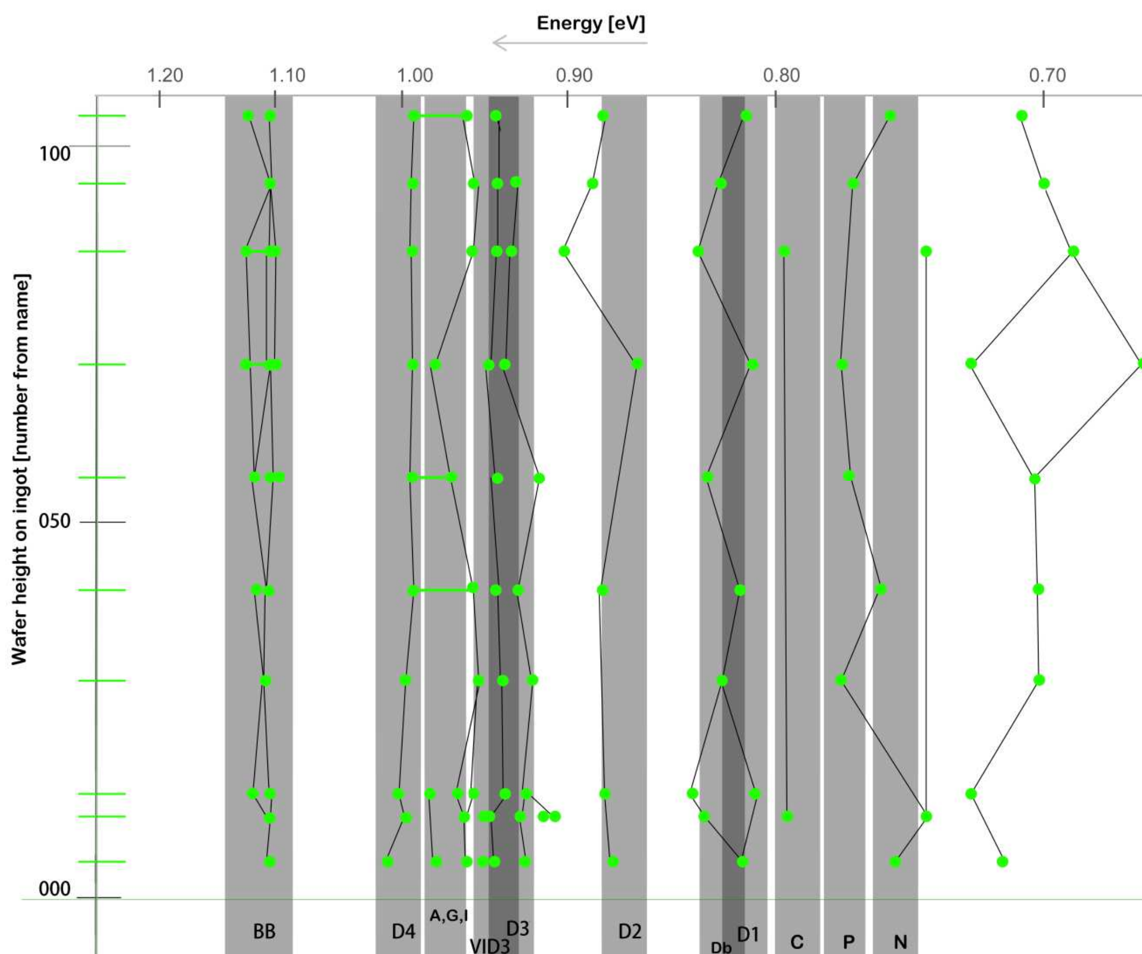

Figure 5.26: Peaks on loadings plots from MCR analysis results of A2+C wafers

Green points are peaks on loadings plots obtained through the MCR analysis of wafers in the A2+C set. Points connected with a green line show energies for a component which showed two peaks on the loadings plot. Black lines connect points which have similar energies. A table with the data points of component peaks is included in the Appendix.

In Figure 5.27 the component peaks for wafers in the HM set are presented. The total number of distinguishable emission signals for this set is in the range 5 -7. This differs from the two previous sets as MCR analysis resulted in a low number of components. There are two possible explenations for this. One is that the material contains a low number of defects, not letting electron-hole pairs recombine through radiative recombination mechanisms. The other possible explenation is that there are a large number of defects, letting electron-hole pairs recombine through a large number of recombination processes, thus reducing the intensity recorded from each of the radiative recombination mechanisms and hindering the MCR analysis in extracting a different component for each signal. The latter explenation, of wafers of low quality, is supported by the fact that BB-PL only showed up in the MCR results for seven of the ten wafers. The BB-PL signal is assumed to be of high intensity in material of good quality.

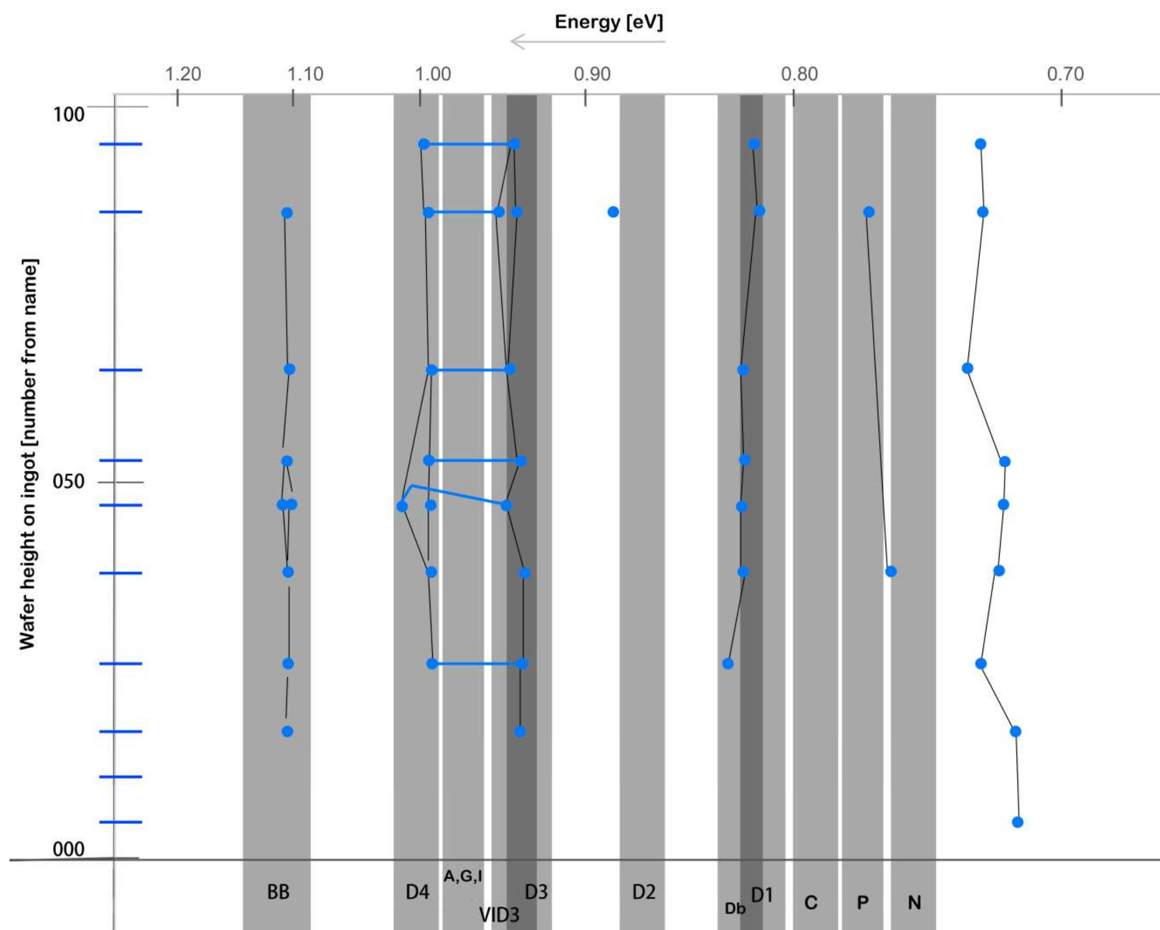

Figure 5.27: Peaks on loadings plots from MCR analysis results of HM wafers
Blue points are peaks on loadings plots obtained through the MCR analysis of wafers in the HM set. Points connected with blue lines show energies for a component which showed two peaks on the loadings plot. Black lines connect points which have similar energies, and connected points vary little in energy. A low number of components were obtained for this set. A table with the data points of component peaks is included in the Appendix.

From the detailed analysis of wafer B2_053 it was shown that the emission signals for BB-PL, for D4 and for D3 were present in large areas of the wafer, while the rest of the signals were mostly point-like.

Although the MCR analysis method has proved to be efficient in separating the different emission signals from the scans of a wafer, there is a possibility that there are more signals present, which the MCR analysis does not effectively extract.

It is important to remember that these results are obtained for unpassivated wafers at 90 K, and are probably different than what would have been obtained at different temperatures or of passivated wafers or cells.

5.3 Comparison between Ingots

The MCR results obtained for the three sets B2, A2+C and HM imaged at 90 K, show a varying number of distinguishable emission signals. In Figure 5.28 the number of significant components found for each wafer in the different sets can be compared. While the B2 set resulted in more components for wafers from a higher position on the ingot, we cannot see the same relationship for the two other sets of wafers. The number of components in Figure 5.28 are the number of components obtained by MCR analysis after subtracting the number of components which are caused by noise. It does not take into account that some components cover several emission signals and some emission signals are erroneously divided into several components. The B2 set are standard wafers, while the HM and A2+C set are HPM wafers.

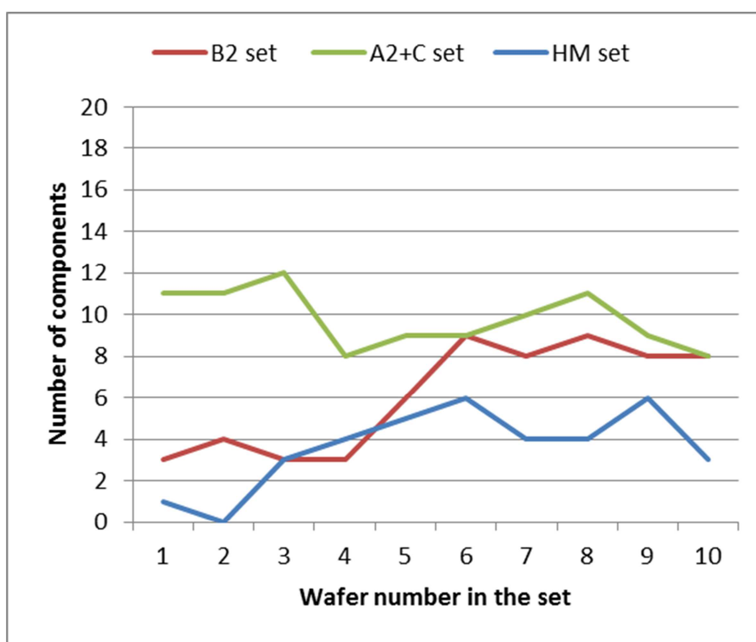

Figure 5.28: Number of significant components in the different sets
The number of components shown here does not include components showing noise. Each of the imaged wafers in a set is given a number based on its position on the ingot. The wafer with origin lowest on the ingot is called wafer number 1.

The energy position of tops on the loadings plots of each wafer were previously shown separately for each set. In Figure 5.29 they are shown together for comparison. In this figure it is possible to compare the three sets and the stability of different signals. Black lines connecting points connect only points belonging to the same set, and are a best guess for which components represent the same emission signal. The point marked with a circle is an example of a component which is assumed to include more than one emission signal, and which has a peak energy position between two known emission signal energies.

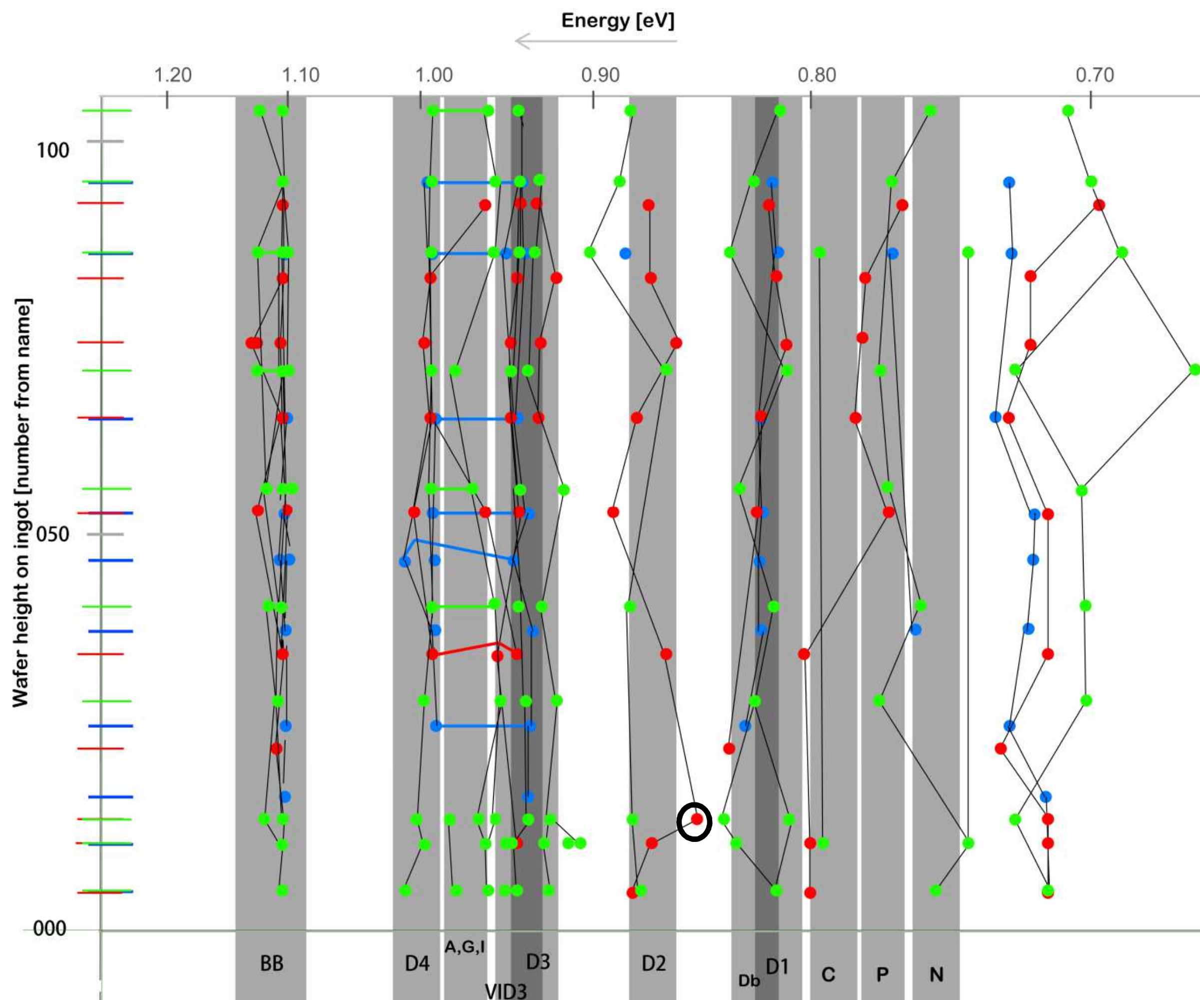

Figure 5.29: Loadings plots peaks from MCR analysis results of wafers in three sets. *The figure shows the position of peaks of different components from the MCR result of each wafer in the B2 set (red), A2+C set (green) and HM set (blue). Connected points in colour are positions of two peaks in one component. Black lines are a guess for which components show the same signal. The data for this figure is a combination of the three tables in the Appendix. The camera can detect emissions with energy in the range of to 0.49 eV – 1.34 eV.*

In Figure 5.29 it can further be seen that the number of components obtained through MCR analysis are most numerous in the range 0.92 – 1.12 eV. In the range 0.92 – 1.0 eV there are several components obtained, making it harder to identify the corresponding signals.

It would be useful to know the impurity and dislocation contents and positions in the samples. This way emission signals could be better identified.

5.4 Room Temperature and RGB Images

5.4.1 Room Temperature Images

Room temperature hyperspectral images were taken of some of the wafers. It was quickly established that the room temperature images carried very little information and gave no results for the MCR analysis other than components showing noise. This is not unexpected, as the wafer samples are unpassivated and at room temperature non-radiative recombination mechanisms will dominate.

5.4.2 RGB Image and Comparison with emission signals

RGB images were taken of the first and the last wafer in the three different sets of wafers with a Cannon camera. The images are shown in Figures 0.1, 0.2, 0.3 and 0.4 of the Appendix. By looking at these images we see that from the bottom towards the top, grain size in the B2 set increases greatly, in the A2+C it stays approximately the same, and in the HM set it increases slightly. This simple visual inspection correlates with the number of significant components found for different wafers in the three series, suggesting that the MCR analysis results in more components for wafers with larger grain size.

When emission signals are compared to the corresponding RGB image, we see that the emission signals are affected by the size and position of the grains. Figures in section E of the Appendix show that some emission signals appear at the grain boundaries, while some signals cover one or several grains. Emissions from the wafers with large grain size have a larger extent than emissions from wafers with small grain size, which all seem point-like.

6 Conclusion

The MCR analysis was an effective method for distinguishing between different emission signals when emission of high intensity was recorded. It was then possible to see the spatial distribution of the different emission signals. The method was not effective at room temperature. We also know that because the wafer samples were unpassivated, measurements were influenced by non-radiative surface recombination. The different emission signals were not picked out for all wafers, and in some cases MCR analysis did not result in a component for BB PL even though BB PL was visible on the image at the corresponding energy.

The number of distinguishable emission signals from different wafers varied. For wafers in the B2 set MCR analysis helped identify eight different emission signals. The MCR analysis for the A2+C set resulted in more components, while for the HM set it resulted in less components.

Those wafers assumed to be of poorest quality showed fewer distinguishable emission signals. A possible explanation is that a large number of recombination mechanisms cause the intensity of signals emitted at different energies to be reduced. Components for wafers showing few distinguishable emission signals are often spectrally wider and seem to cover a range of what are several components in other wafers.

Components covering large areas on the wafer are BB PL, D4 and D3. As expected, D4 and D3 originate at approximately the same areas. The component obtained for the D4 signal showed an additional peak at 0.96 eV. The D4 emission signal and the additional peak were only divided into two separate components for one of the ten wafers. Point-like emissions are separated into signals at 0.94 eV, 0.92 eV (D2), 0.82 eV (D1?), 0.77 eV and 0.72 eV. While the signal for D2 was identified, the identification of the corresponding emission lines with the remaining signals is of great uncertainty.

As this master's thesis deals with unpassivated wafers, surface recombination has a large effect on the measurements. Higher surface recombination leads to lower radiative SRH recombination, reducing the intensity of recorded signals.

Not much is known about the production process of the wafers. By knowing more, more conclusions can be drawn on which lines from the literature it is that we see. A strength of the utilised setup is the availability of several wafers from the same ingot, allowing the comparison between similar wafers.

Although there was some uncertainty as to the number of components chosen in the MCR analysis, and that it might divide one signal into several components, this rarely happened for wafers in the B2 set. For the most part it happened for the BB-PL, which is easily identifiable anyway. On the contrary, there seem to be components which are spectrally wider and seem to not have been divided into enough components.

6.1 Further Research

Further research in this project is needed to bring more understanding about the different PL signals. Suggested research includes doing similar experiments again, or comparing PL results with measurements obtained through other characterisation methods.

When repeating the experiment, suggested changes are doing measurements at different temperatures, doing measurements on more than ten wafers from the same ingot, to do the experiment either with cells made from neighbouring wafers or with the same wafers after passivation. Also, increasing the resolution by moving the sample closer to the camera or trying different statistical analyses would be interesting.

It would also be interesting to compare results obtained by a similar method with results obtained by other methods, including knowledge about the production method and results of material characterisation by other methods.

References

1. Chen, C.J., *Physics of solar energy*. 2011, Hoboken, N.J.: Wiley. pp. 1, 161-207.

2. Green, M.A., *Solar cells: operating principles, technology and system applications*. 1992, Kensington: University of New South Wales. pp. 1- 135.

3. Callister, W.D. and D.G. Rethwisch, *Fundamentals of materials science and engineering: an integrated approach*. 2013, Singapore: Wiley. pp. 483-515.

4. Hull, D. and D.J. Bacon, *Introduction to dislocations*. 2011, Amsterdam: Elsevier. pp. 1-20.

5. Sauer, R., et al., *DISLOCATION-RELATED PHOTOLUMINESCENCE IN SILICON.* Applied Physics a-Materials Science & Processing, 1985. 36(1): pp. 1-13.

6. McHedlidze, T., et al., *Capability of photoluminescence for characterization of multi-crystalline silicon.* Journal of Applied Physics, 2012. 111(7): p. 11.

7. Trupke, T., J. Nyhus, and J. Haunschild, *Luminescence imaging for inline characterisation in silicon photovoltaics.* Physica Status Solidi-Rapid Research Letters, 2011. 5(4): pp. 131-137.

8. Johnston, S., et al., *Comparison of Photoluminescence Imaging on Starting MultiCrystalline Silicon Wafers to Finished Cell Performance*. 2012 38th IEEE Photovoltaic Specialists Conference. 2012, New York: IEEE.

9. Johnston, S., et al., *Quality Characterization of Silicon Bricks using Photoluminescence Imaging and Photoconductive Decay*. 2012 38th IEEE Photovoltaic Specialists Conference. 2012, New York: IEEE.

10. Arguirov, T., et al., *Photoluminescence study on defects in multicrystalline silicon.* Semiconductors, 2007. 41(4): pp. 436-439.

11. Binetti, S.L., A.; Sassella, A, *Photoluminescence and infrared spectroscopy for the study of defects in silicon for photovoltaic applications.* Solar Energy Materials and Solar Cells, 2014. http://dx.doi.org/10.1016/j.solmat.2014.02.004.

12. Flo, A., et al., *Distribution of radiative crystal imperfections through a silicon ingot.* Aip Advances, 2013. 3(11): p. 9.

13. Mudryi, A.V., et al., *Impurities and defects in multicrystalline silicon for solar cells: low-temperature photoluminescence investigations.* Solar Energy Materials and Solar Cells, 2002. 72(1-4): pp. 503-508.

14. Tajima, M., et al., *Photoluminescence Analysis of Iron Contamination Effect in Multicrystalline Silicon Wafers for Solar Cells.* Journal of Electronic Materials, 2010. 39(6): pp. 747-750.

15. Tajima, M., et al., *Deep-level photoluminescence due to dislocations and oxygen precipitates in multicrystalline Si.* Journal of Applied Physics, 2012. 111(11): p. 6.

16. Inoue, M., et al., *Microscopic and spectroscopic mapping of dislocation-related photoluminescence in multicrystalline silicon wafers.* Journal of Materials Science-Materials in Electronics, 2008. 19: pp. S132-S134.

17. Schubert, M.C., et al., *Analysis of performance limiting material properties of multicrystalline silicon.* Solar Energy Materials and Solar Cells, 2010. 94(9): pp. 1451-1456.

18. Arguirov, T., et al., *Temperature behaviour of extended defects in solar grade silicon investigated by photoluminescence and EBIC.* Materials Science and Engineering B-Solid State Materials for Advanced Technology, 2003. 102(1-3): pp. 251-256.

19. Yang, Y.M., et al., *Development of high-performance multicrystalline silicon for photovoltaic industry.* Progress in Photovoltaics: Research and Applications, 2013.

20. Giesecke, J.A., et al., *Spatially Resolved Characterization of Silicon As-Cut Wafers with Photoluminescence Imaging.* Progress in Photovoltaics, 2009. 17(4): pp. 217-225.

Appendix

A. RGB Images of Fist and Last Wafers in each wafer set

Figure 0.1: RGB image of wafer B2_005.
The RGB image of wafer B2_005 shows that the crystal grains in the wafer are small and numerous. The printed name of the wafer can be seen in the upper left corner. The dimensions of the wafer are 15.6 x 15.6 cm. Light and dark areas are due to lighting conditions and are not of interest.

Figure 0.2: RGB image of wafer B2_092.
The RGB image of wafer B2_092 shows that the crystal grains in the wafer are large and few. The printed name of the wafer can be seen in the upper left corner. The dimensions of the wafer are 15.6 x 15.6 cm. Light and dark areas are due to lighting conditions and are not of interest.

Figure 0.3: First and last wafer in A2+C set
Wafer A2+C_005 at the top and wafer A2+C_104 at the bottom. Both wafers show approximately the same grain size.

Figure 0.4: First and last wafer in HM set
Wafer HM_005 at the top and wafer HM_095 at the bottom. Wafer HM_095 shows slightly larger grain size than wafer HM_005.

B. Example of Components Showing Noise for Wafer B2_053

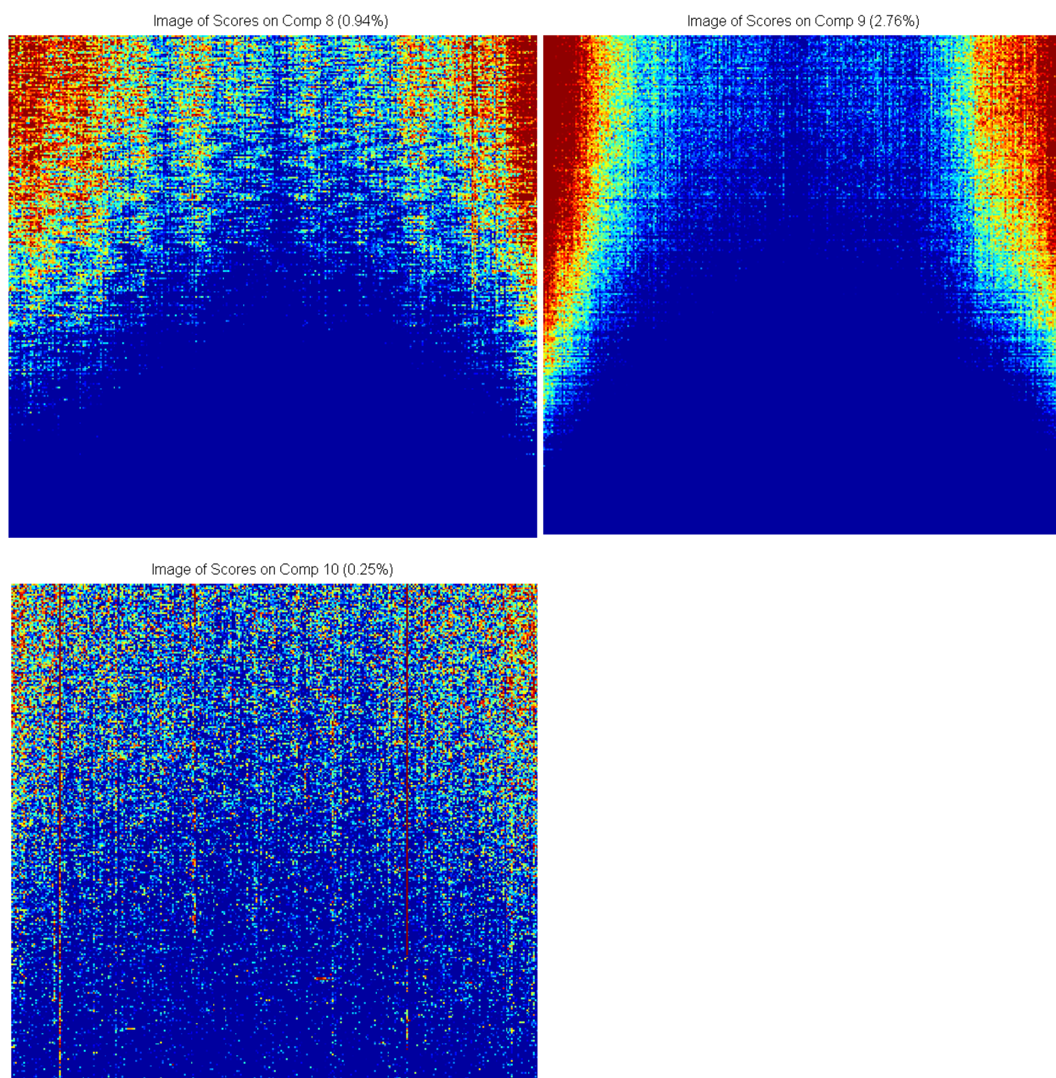

Figure 0.5: Scores for components showing noise
Different examples of components showing noise. These are components number 8, 9 and 10 from the results of the MCR analysis of wafer B2_053.

C. Images Showing Component Pairs for Wafer B2_053

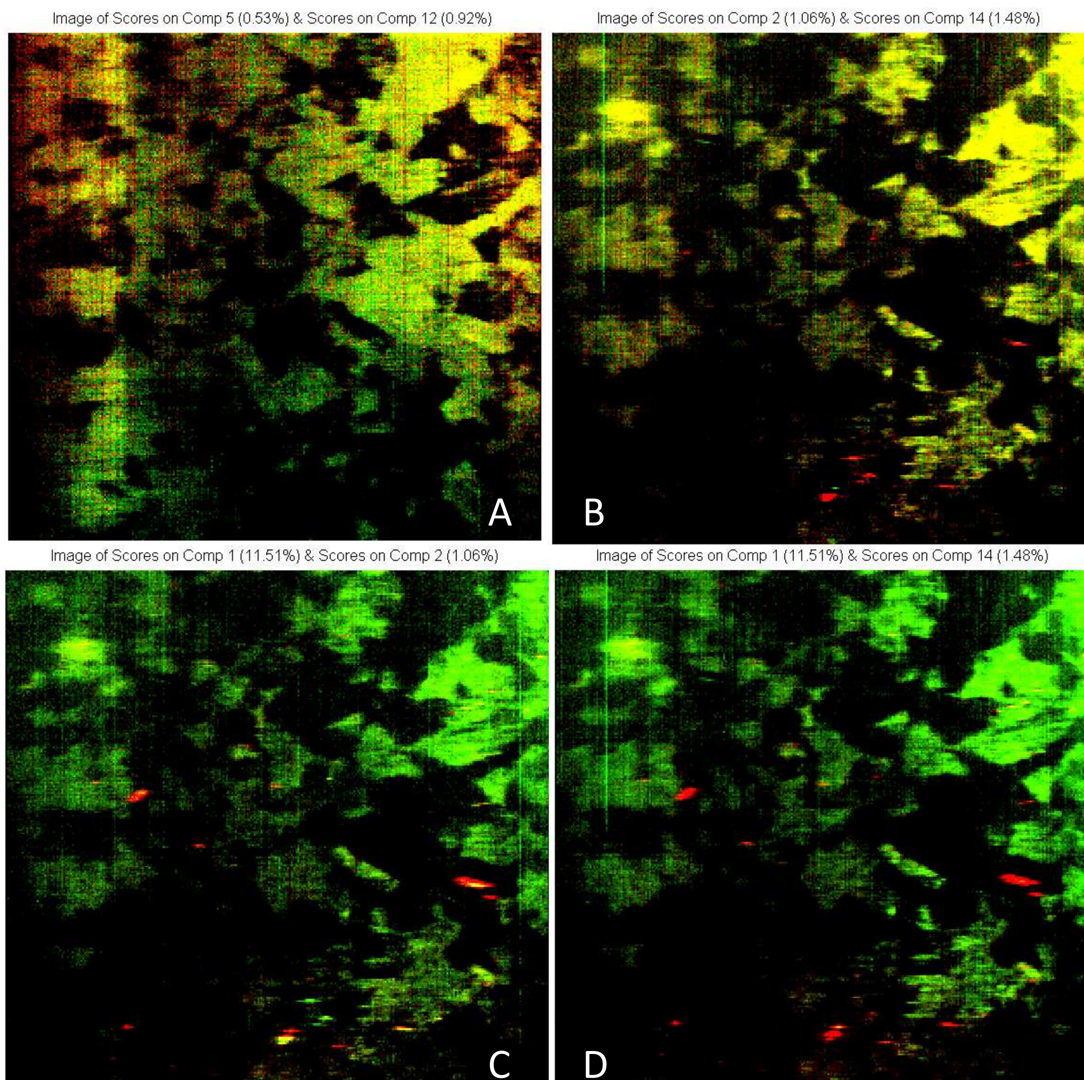

Figure 0.6: Component pairs for wafer B2_053 (1)

Image A shows component 5 (red) and 12 (green): These two components blend into each other. Image B shows component 2 (red) and 14 (green): Large areas are covered by both components, while points are only shown by component 2 in red. Image C shows component 1 (red) and 2 (green). Image D shows component 1 (red) and 14 (green). Yellow areas are areas where both components are present. Image C and D show components with very different spatial distributions.

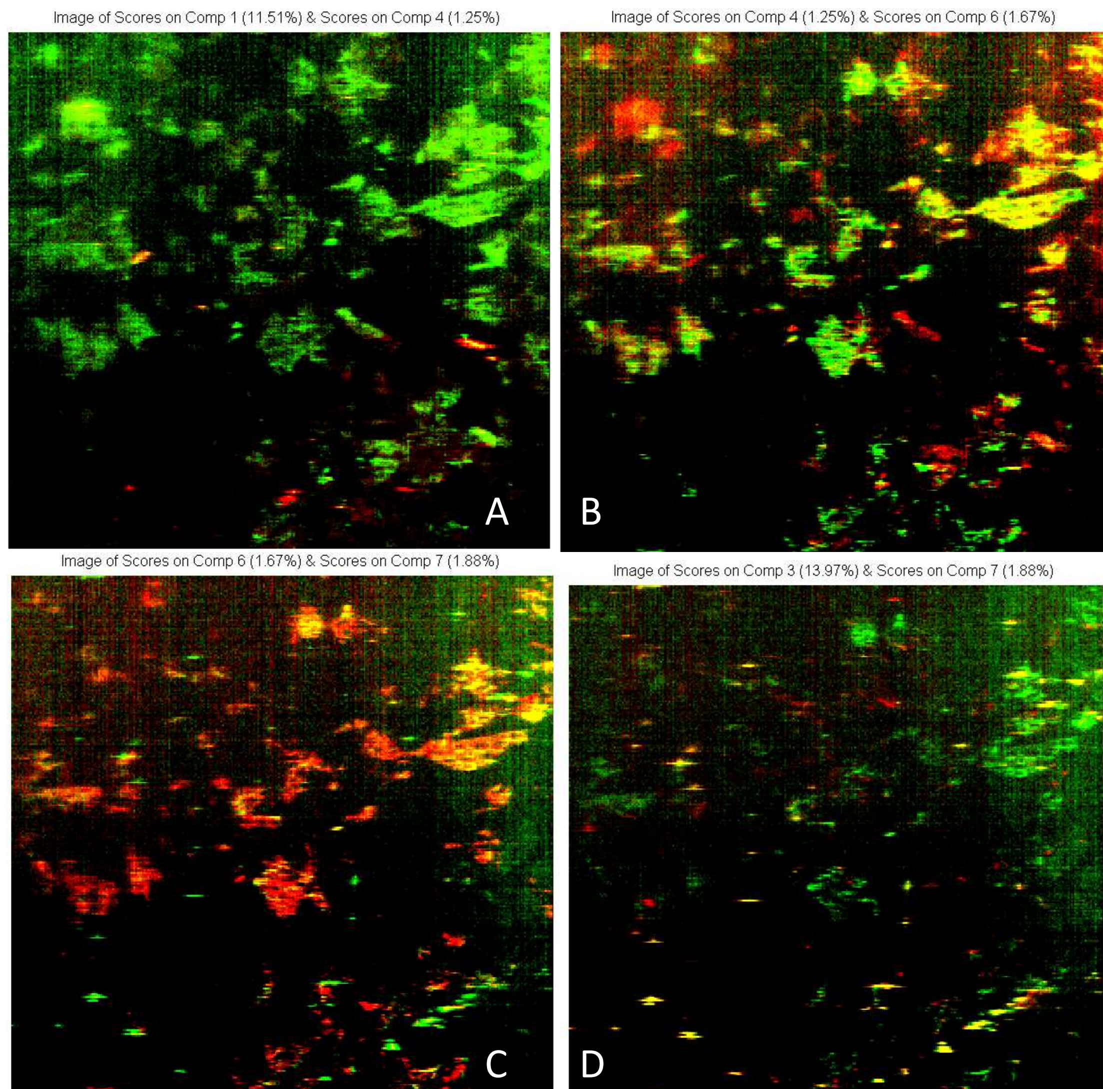

Figure 0.7: Component pairs for wafer B2_053 (2)

Image A shows component 1 (red) and 4 (green). Image B shows component 4 (red) and 6 (green). Image C shows component 6 (red) and 7 (green). Image D shows component 3 (red) and 7 (green). Yellow areas are areas where both components are present. All four images show component pairs which are present in some common areas and some separate areas.

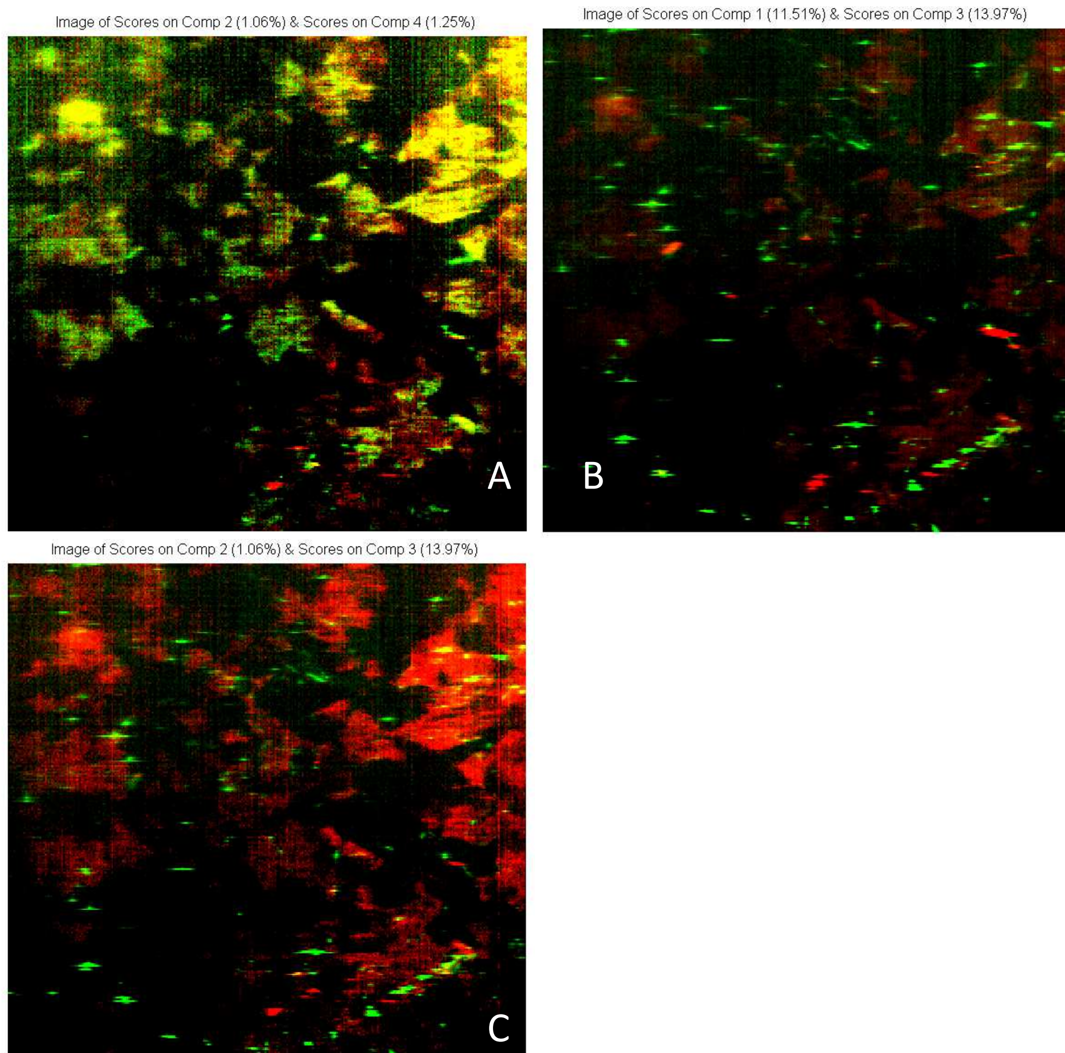

Figure 0.8: Component pairs for wafer B2_053 (3)

Image A shows component 2 (red) and 4 (green). They are present in some common areas but also in separate areas. Image B shows component 1 (red) and 3 (green). Image C shows component 2 (red) and 3 (green). Both image B and C show component that are present in mostly different areas.

D. Tables of Values in Figures 5.13, 5.26, 5.27

Wafer number										
005							77		100	130
011					63		80		100	130
014	33						84			130
023	33							90		125
035	33		54-69		63		80		100	130
053	30	33	50	59	63		76	95	109	130
064	33		52		62	66	78	90	105	125
074	32	33	51		62	66	84	96	109	125
083	33		52		63	68	80	94	109	130
092	33		59		63	66	76	97	110	135

Table 0.1: Band number of loadings peaks in B2 set
The band at which different components peak on the loadings plots obtained through MCR analysis of wafers in the B2 set. Number indicates band number.

Wafer number													
005	33		49	55	59	61	64	67	79		95	106	130
011	33		51	59	61	62	66	69	71		91	103	120
014	31	33	50	54	58	60	64	67	77	88	97		126
029	32			51		61	64	68			93		135
041	31	33		52-60		63	66		77		95	114	135
056	31	33	34	52-57		63	68				91	111	135
071	30-34	33		52-55		62	64		82	97	109	126	150
086	30-34	33		52		60	63	65	72	90	101	120	140
095	33			52		60	63	66	76	93	111	136	
104	30	33		52-59		63			77	96	115	133	

Table 0.2: Band number of loadings peaks in A2+C set.
The band at which different components peak on the loadings plots obtained through MCR analysis of wafers in the A2+C set. Number indicates band number.

Wafer number						
005						130
011						
017	33		64			130
026	33		52-64		91	125
038	33		52	64	93	128
047	32	33	48-62	52	93	128
053	33		52-64		94	128
065	33		52-62		93	123
086	33		52-61	63	95	125
095			51-63		95	125

Table 0.3: Band number of loadings peaks in HM set.
The band at which different components peak on the loadings plots obtained through MCR analysis of wafers in the HM set. Number indicates band number.

E. Comparison of Emission Signals and Positions on Wafers

E.1. Wafer B2_005

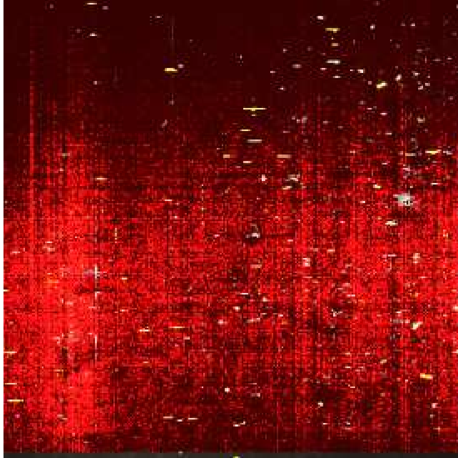

Figure 0.9: MATLAB extracted emissions overlaid on one image of wafer B2_005
BB-PL is shown in red. All other DRL signals are shown in white and yellow.

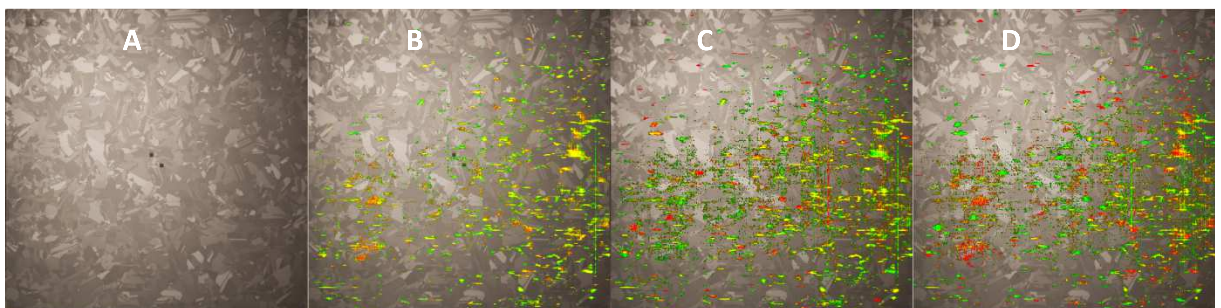

Figure 0.10: Scores images overlaid on RGB images of wafer B2_005
The figure shows A) no emissions; B) 0.87eV in red and 0.80eV in green; C) 0.71eV in red and 0.80eV in green; D) 0.87 eV in red and 0.71eV in green. Yellow areas are common for both components.

E.2.Wafer B2_092

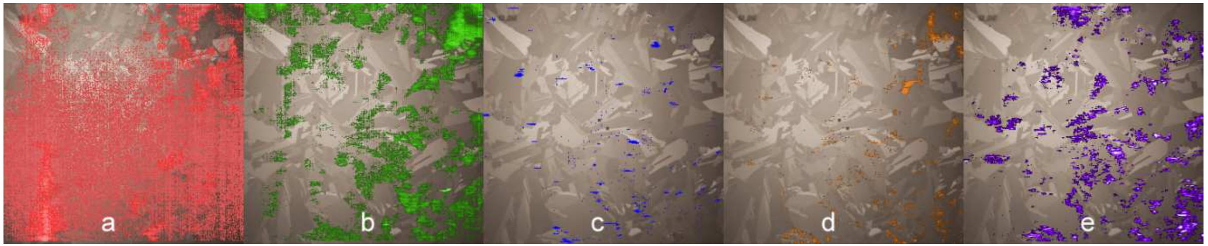

Figure 0.11: MATLAB extracted emissions overlaid on image of wafer B2_005
The RGB image for wafer B2_005 is shown 5 times (a-e), overlaid with different emission signals. a) shows BB PL, b) shows D4, c) shows VID3, d) shows D2 and e) shows D1.

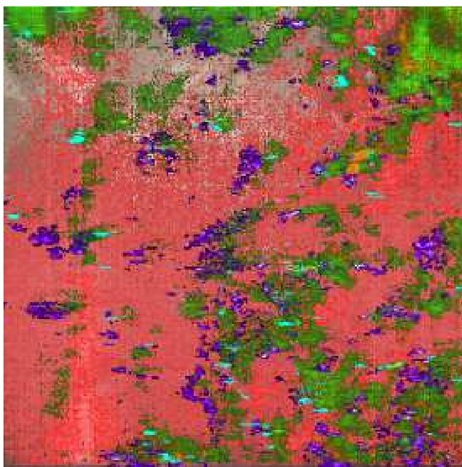

Figure 0.12: MATLAB extracted emissions overlaid on one image of wafer B2_092
The colours and emission signals are the same as in Figure 0.12, but all signals are overlaid on one image, allowing the position of the signals to be more easily compared.

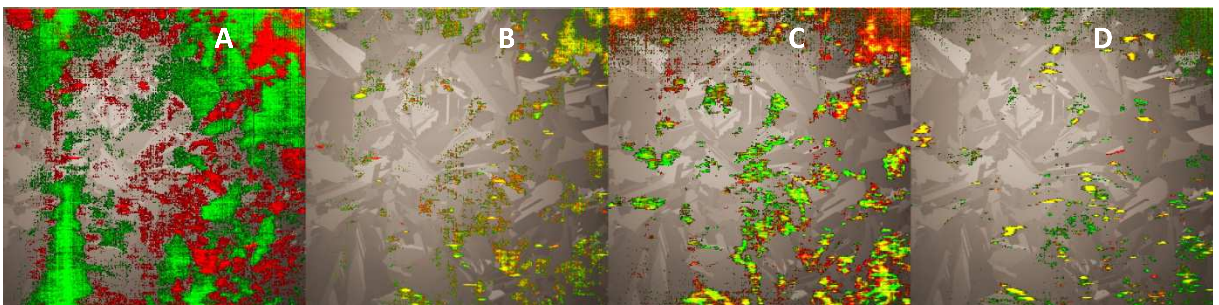

Figure 0.13: Scores images overlaid on RGB images of wafer B2_092
The figure shows A) BB in green and D4+0.96eV inred; B) 0.94eV in red and D3 in green; C) D2 in red and 0.82eV(D1+Db) green; D) 0.77eV in green and 0.72eV in red. Yellow areas are common for both components.

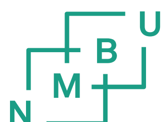

Norwegian University
of Life Sciences

Postboks 5003
NO-1432 Ås, Norway
+47 67 23 00 00
www.nmbu.no